Microclimatic Effects of Forest to Peatland Transitions Within the Boreal Plains

by

Adam John Green

A thesis

presented to the University of Waterloo

in fulfilment of the

thesis requirement for the degree of

Master of Science

in

Geography

Waterloo, Ontario, Canada, 2019

Author's Declaration

I hereby declare that I am the sole author of this thesis. This is a true copy of the thesis, including any required final revisions, as accepted by my examiners.

I understand that my thesis may be made electronically available to the public.

Abstract

Peatlands cover approximately 50% of the total landscape of the Western Boreal Forest, which includes the sub-humid Boreal Plains (BP) ecozone. The BP experiences persistent water deficit conditions, promoting anaerobic conditions, which has the potential to increase decomposition, transforming the peatlands from carbon sinks to carbon sources. With evapotranspiration (ET) being the dominant source of water loss in the BP, peatland persistence is hydrologically precarious, and as such, it is necessary to understand the dynamics and controls on ET within these systems. Due to the heterogeneity of the landscape, surrounding upland forests often shelter peatlands from wind. This results in spatially varying evaporative rates, which can influence surface moisture and vegetation regimes across a peatlands surface. High-resolution turbulent models allow for such flow scenarios to be resolved as they resolve flow in a 3D domain. Therefore, high-resolution turbulent models are essential in assessing the spatial variability of stresses placed on surface scalars such as ET, by displacement height transition.

This study uses a canopy resolving large-eddy simulation (RAFLES) to study the impact of displacement height transitions on surface-atmosphere exchanges of moisture within peatlands of the BP. The dimensions, vegetation structure and energy dynamics of the modeled peatlands were generated from observations of natural peatlands of the BP. Within the sheltered region leeward of a backward-facing step transition, the simulated peatlands experienced higher resistances to surface-atmosphere exchanges of moisture when compared to the reattachment and recovery regions. However, this trend was muted when the surface roughness of the peatland was increased as the roughness lowered the overall resistance of the surface. This study also found that the length of the peatland did not influence the flow reattachment dynamics within the peatland. However, it was observed that the peatlands with a narrow shape and a curved front-facing step geometry resulted in faster regional wind velocities. Understanding the turbulent dynamics within heterogeneous landscapes can help to control the rate and variability of surface to atmosphere exchanges of moisture within disrupted and reclaimed landscapes which can increase the predictability of moisture demands within future landscapes.

Acknowledgments

I have received endless support from many people that has led to the completion of this thesis. First, and foremost, I would like to thank Dr. Richard Petrone for not only the opportunity, support, and insight but also the confidence and freedom to shape my research the way I saw fit. Thank you to Dr. Gil Bohrer for providing me with the opportunity and assistance needed to use RAFLES, as well as all of the insightful edits along the way.

To all of the members of the Hydrometeorology Research Group: Thank you for all of the friendships that have been made and for sharing in this experience with me. A special thanks to George Sutherland for all of the field equipment setup, maintenance, and data processing that occurred along the way - and for taking the time to educate me on all of the field sites, equipment and for always being a phone call away. Thank you to Dylan Harch, Patrick Pow, Kate Jamieson and Timothy Morin for their assistance in the field, lab or with coding help. I would also like to thank Eric Kessel, James Sherwood, and Tristan Gingras-Hill for their assistance and camaraderie in the field and throughout my time working on this project.

This research would not have been possible without the support and contributions form Natural Sciences and Engineering Research Council of Canada, Northern Scientific Training Program, Esso Imperial Oil Ltd., Shell Canada Ltd., Suncor Energy Inc., Syncrude Canada Ltd., Ducks Unlimited and the Ohio Supercomputing Center for their funding contributions.

Lastly, and most importantly, I would like to thank my Mom, Dad, and Sisters who have provided me with unwavering support and motivation throughout my academic tenure. The constant questions of when will you be finished your thesis has finally come to its conclusion.

To my loving family:

Susan, Gordon, Allison and Erin Green

I could not have done this without your love and support.

Thank you.

Table of Contents

List of Figures

List of Tables

1.0 Introduction:

The Boreal Plains (BP) of the Western Boreal Forest (WBF) is a mosaic of wetlands, small surface water bodies, and aspen (*Populus Tremuloides* and *Populus Balsamifera*) dominated uplands. Within the BP, wetlands account for approximately 50% of the natural landscape, of which ~90% are peatlands (Vitt et al., 1996). The defining characteristics of Canadian peatlands are that they: 1) are peat accumulating; 2) have a peat depth greater than 40 cm; and 3) have a water table at or near the ground surface (National Wetlands Working Group, 1997). Peat accumulation is a result of the imbalance in net primary production (NPP) (Bridgham et al., 1996) as a result of high vegetation productivity, and reduced decomposition rates produced by anaerobic conditions caused by the persistently high water table (Clymo, 1965; Maimer, 1986; Farrish and Grigal 1988; Vitt, 1990; Thormann et al., 1999; Vitt et al., 2009; Rydin and Jeglum, 2006). Consequently, peatlands are a net sink of CO_2 and represent the largest carbon pool in Canada (Gorham, 1991). Climactically, the BP is situated in a sub-humid climate where persistent water deficit conditions result from potential evapotranspiration (PET) is greater than precipitation (P) on an annual basis (Devito et al., 2005; Ketcheson and Price, 2016) where wetlands are sustained by infrequent wet years that occur on a 10 - 15 year cycle (Marshall et al., 1999; Devito et al., 2005). Despite the seasonal water deficit conditions of the region, peatlands are still a prominent feature across the BP (Ferone and Devito, 2004; Petrone et al., 2007). Previous research on the hydrologic and microclimatic functioning of perched peatlands has shown that these systems have negative autogenic feedbacks such as turbulent sheltering, radiative sheltering and vegetative controls (Petrone et al., 2007; James, 2017; Waddington et al., 2015). These feedbacks may increase the resiliency of such peatlands to evaporative losses by changing the ratio of P to PET within the peatland (Petrone et al., 2007; Waddington et al., 2015; Hokanson et al., 2016; James, 2017).

Evapotranspiration (ET) is the combination of both evaporation (E) from the surface and transpiration (T) from plants (Oke, 1988). ET is an important component of both the water budget of terrestrial ecosystems (Brutsaert, 1982) and energy budget (Oke, 1988). Penman (1948) stated that three conditions are required in order for E to occur: 1) water must be present; 2) there must be enough energy to induce a phase change of liquid to vapor; and 3) water vapor entering the atmosphere immediately above the surface must be transported away from the surface. Peatlands of the BP typically have high water tables, which satisfies the water avaiablility and can result in evaporative rates comparable to open water bodies (Nichols and Brown, 1980). However, when the water table drops below 30 cm ET rates from non-vascular vegetation can drop considerably as the evaporative demand cannot be met as the supply of water to the surface is restricted by the rate of capillary rise of the peat (Price 1997, Golubev and Whittington, 2018). Although vascular vegetation has access to deeper water tables, T losses are regulated by their roots, internal water-transport systems, and stomata (Baldocchi et al., 1991; Mitsch and Gosselink, 2000; Chapin et al., 2002). Stomata dynamics are controlled by such factors as soil moisture, incoming radiation, vegetation LAI, vegetation height, temperature, and differences in CO_2 concentration and vapour pressure between the atmosphere and the inside of the leaf (Baldocchi et al., 1991; Collatz et al., 1991; McNaughton and Jarvis, 1991; Chen et al., 1999b; Chapin et al., 2002; Raddatz et al., 2009; Jassal et al. 2009).

Increased anthropogenic disturbances from oil and gas extraction, and forestry development have resulted in the disruption to the BP ranging from individual ecosystem impacts to the scale of entire landscapes (Alberta Environmental Protection, 1998; Johnson and Miyanishi, 2008; Government of Alberta, 2015). The Athabasca Oil Sands Region (AOSR) is the third largest proven oil deposit (166 billion barrels as of 2014) in the world (Alberta Government, 2015;

Woynillowicz et al., 2005). It is estimated that 4,800 km^2 of the AOSR is accessible for near surface (~ 75 m) open-pit surface mining extraction, while deeper deposits require steam assisted gravity drainage techniques (SAGD) (Alberta Government, 2015). As of 2018, oil-sands development has been estimated to have disturbed more than 901 km^2 (Canadian Oil and Natural Gas Producers, 2018). Such disturbances require land and water reclamation projects at a landscape scale to satisfy mine closure plans. Legislation mandates that the land is returned to an equivalent and functioning land class, i.e., the mosaic of peat-accumulating wetlands and forests (Daly et al., 2012). At a smaller scale, forestry activities typically use the cut-block technique where selected strips of forests are completely harvested. Such activities alter the natural landscape at the point of disturbance (Amiro et al., 2006; Petrone et al., 2015; Whitson et al., 2005; Carrera- Hernández et al., 2011; Plach et al., 2016), as well as the surrounding ecosystems by fragmenting the landscape and modifying the hydrological stability of the region through alteration of the regional microclimate (Solondz et al., 2008; Brown et al., 2010; Petrone et al., 2007). Due to the hydrologic sensitivity of the BP and the combined economic, and legal requirements associated with anthropogenic activities, it is advantageous to investigate landscape modifications that can influence the resiliency and stability of this ecozone. Therefore, it is critical to understand atmospheric transport processes and boundary layer interactions within this complex landscape as changes to these processes may modify the hydrological balance of the region.

The heterogeneous mosaic of peatlands, upland forests and anthropogenic disturbances that comprise of the BP results in sharp transitions in displacement heights that produce complex transitional flows and turbulent processes (Bou-Zeid et al. 2004; Markfort et al., 2010). Studies investigating flow separation over heterogeneous surfaces (e.g. Patton et al. 1998; Belcher et al. 2003; Yang et al. 2006b; Cassiani et al. 2008; Dupont and Brunet 2008a; Fontan et al. 2013;

Chatziefstratiou et al., 2014) have identified transition structures by using the "step analogy" where there is either a forward-facing (FFS) or a backward-facing step (BFS) depending on the wind direction, with discussions being primarily focused on either the approaching or exiting flow (Detto et al. 2008; Panferov and Sogachev 2008; Chatziefstratiou et al., 2014). In complex terrain such as the BP, such surface simplifications can be combined with a sequence of transitions such as BFS – Gap – FFS (e.g., a peatland surrounded by a forest), and can be conceptualized by combining and modifying the frameworks developed by Judd et al. (1998), Cleugh (1998) and Belcher et al. (2003) as shown in Figure 1-1.

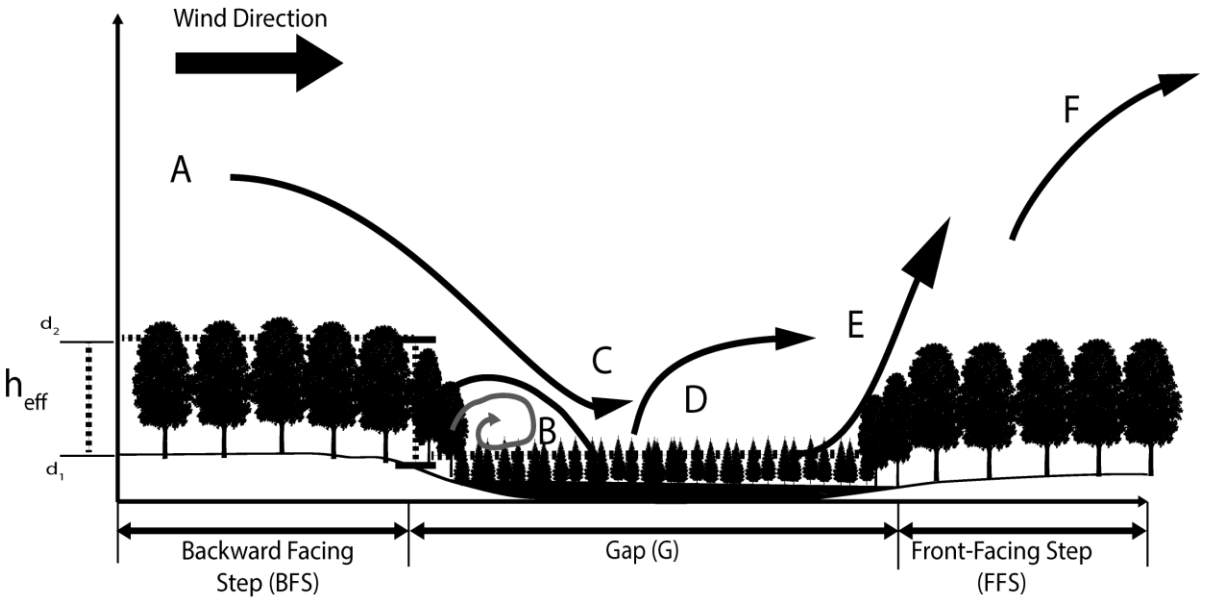

Figure 1-1: Schematic showing the unique zones created by flow adjusting over a backward facing step (BFS) transition, identifying the successive regions in the flow path: (A) approach flow; (B) sheltered region; (C) reattachment zone; (D) recovery region, (E) uplift region; (F) roughness change region (IBL).

Backward Facing Step Flow Dynamics:

Turbulent stresses vary across the gap surface as a result of the flow regimes produced by the displacement height transitions (Figure 1-1). The turbulent state of the *approach flow* (A in Figure 1-1) has been shown to influence the lengths and characteristics of the *sheltered region* (B in Figure 1-1) and *reattachment zone* (C in Figure 1-1) (Simpson, 1989; Castro and Epik, 1998, Markfort et

al., 2014; Chatziefstratiou et al. 2014; Kindere and Ganapathisubramani, 2018). For example, high approach flow turbulence has been shown to decrease the reattachment distance, having a larger impact on the reattachment distance compared to the Reynolds number and perturbation strength (Adams & Johnston, 1988; Piirto et al., 2003) for both a BFS and FFS transition (Isomoto & Honami, 1989; Essel, Mali, Tahcher, & Tachie, 2014). The sudden change in the displacement height results in a decoupling of the flow profile from the surface, increasing flow velocities and wind shear as it adjusts to the new surface element. The decoupling of the flow profile produced a region of reduced flow that is separated from the adjusting layer above (B in Figure 1-1), which results in a *sheltered region* where turbulent transport is reduced resulting in increased scalar concentrations (Mcnaughton, 1988; Chapter 2). When mean *flow reattaches* with the surface layer (C in Figure 1-1), it typically has high flow velocities and turbulent stresses that produce an adverse pressure gradient resulting in flow reversals within the sheltered region. The development of a flow profile ensues after flow reattachment occurs, as the *flow recovers* (D in Figure 1-1) and surface turbulence equilibrates to the new surface layer and its roughness elements resulting in homogenous mixing of the surface layer.

Front Facing Step Flow Dynamics:

As flow approaches the FFS, it is assumed the flow is in a developed logarithmic flow profile. The *uplift region* (E in Figure 1-1) is characterized by high vertical wind speeds that lifts flow above and out of the step transitions, which has been shown to effectively eject particles and scalars from the surface and into the atmosphere (Bergen, 1975; Goodrick et al., 2013; Belcher et al., 2008; Pruegor et al., 2008). The uplift region is often followed by a stagnation region upwind of the FFS, where flow velocities and turbulence subside (Wang and Tackle, 1995). However, depending on the porosity of the FFS, this stagnation point can greatly vary in strength and size with FFS porosity

- where higher porosities result in decreased flow stagnation (Wang and Tackle, 1995). Above the FFS, the flow enters the *roughness change region* (F in Figure 1-1) where the flow adjusts to the roughness length of the new surface as an internal boundary layer (IBL) develops. However, the length of the FFS surface and the state of the adjusting flow can influence downwind structures; Van der Kindere and Ganapathisubramani (2018) observed that when the length of the FFS was too short to allow for flow recovery, the BFS downwind had a significantly longer reattachment region.

Due to the complexities of displacement height transitions, single point eddy-covariance (EC) measurements are difficult to interpret and neglect the theoretical assumptions of the eddy-covariance method. These assumptions consist of, but are not limited to: 1) the sensors observe a homogeneous surface layer; 2) zero mean vertical flow; and 3) no vertical divergence of fluxes (Yang et al., 2006a; Lee, 2000; Paw et al., 2000). Due to the complexities of field measurements, 3-D computational fluid dynamic models that can resolve turbulence at a forest-to-peatland transition can be used to improve the understanding of flow dynamics within such environments (Bohrer et al., 2009).

The reduction of computational costs has seen the emergence of Large Eddy Simulations (LES) as a viable research tool. However, many studies use simplified structures such as transitions from blocks to flat surfaces or simplified canopy structures that assert drag on the mean flow. Currently, semi-porous forest canopies are being modeled with the aid of computationally competent platforms and the ability to integrate vegetation profiles into LES has become available in models such as Regional Atmospheric Forest Large Eddy Simulation (RAFLES) (Bohrer et al., 2009) via the Virtual Canopy Generator (V-CaGe) (Bohrer et al., 2007). RAFLES Canopy representation includes a multi-layer, 3-D heterogeneous canopy, where each canopy-containing

voxel is prescribed with volume and aperture restriction to the flow due to the presence of modeled trees, and leaf density that exerts drag on the flow and acts as a source of heat and water vapor fluxes (Bohrer et al. 2009). Volume and aperture restrictions interact with the numerical solution of the flow following the shaved grid-cell method (Adcroft et al., 1997; Bohrer et al., 2009). Allowing canopy integration into LES gives us with the ability to accurately model complex flow transitions as it has been observed that canopy elements can a significant influence the turbulent dynamics of transition flow (Markfort et al., 2014; Chatziefstratiou et al., 2014).

RAFLES has been used in several recent studies used to model synthetic landscapes to gain a better understanding of complex natural phenomena. For example, Chatziefstratiou et al. (2014) used RAFLES to investigate the impact that canopy porosity has on the flow around a block structure which represented both an FFS and BFS. Chatziefstratiou et al. (2014) found that flow around these transitions was sensitive to porosity itself and how the model represented the porosity either it be from volume or aperture restrictions or both. RAFLES has also been used in other studies looking and flow transitions where Kenney et al. (2017) investigated how flow interacts within a pond surrounded by a forest which represents a BFS-Gap-FFS and its impact on the validity of the eddy covariance method within these regions. Kenney et al. (2017), found that these transition regions influenced flow and the resulting divergence of fluxes from the pond surface, however, they did suggest that a lower EC measurement height and tower placement can reduce the interference that the transition has on the measurements.

1.1 Research Objectives and Format

Turbulent sheltering of wetlands through surface transitions within the landscape mosaic of the BP may be important control on atmospheric water losses from these systems in the sub-humid climate. Further, surface heterogeneity within the BP produces complex flow patterns that make it

difficult to estimate scalar fluxes as such flow patterns defy the general assumptions of the eddy covariance method. In order to understand the flows within such landscapes, I made use of the RAFLES to resolve turbulent flow and the resultant scalar fluxes. Therefore, the goal of this paper is to investigate how flow separation affects turbulence and evaporative stresses within peatlands of the BP, and the primary research objectives of this study are to:

1. Characterize the impact of flow separation on microclimates and evaporative stresses within peatlands of the BP;
2. Asses the influence that peatland surface roughness and fetch length have on turbulence and microclimates within a peatland of the BP;
3. Comment on the impact of peatland design and landscape configuration on turbulent processes within a peatland and at a regional scale and how it can influence land management strategies.

This manuscript style thesis comprises two individual research papers. The first manuscript examines the influence that BFS flow transitions and peatland surface roughness have on peatland microclimates and evaporative stresses. The second manuscript focuses on the implications that fetch length has on flow separation and micrometeorological dynamics within a peatland, furthermore, this study addresses the effects that peatland geometry and FFS shape have on within peatland and regional flow dynamics.

2.0 Microclimatic Effects of a Forest to Peatland Transition on Aerodynamic Resistance to Evapotranspiration in the Boreal Plains

2.1 Introduction

The Boreal Plains region (BP) of the Western Boreal Forest (WBF) is a complex mosaic of wetlands and aspen dominated uplands, where wetlands account for approximately 50 % of the natural landscape; peatlands comprise 90% of these wetlands (Vitt et al., 1996). The sub-humid climate of the BP results in persistent water deficit conditions where potential evapotranspiration (PET) is greater than precipitation (P) on an annual basis with wetlands being sustained by infrequent wet years on a 10 - 15 year cycle (Marshall et al., 1999; Devito et al., 2005). Peatlands of the BP, and the WBF as a whole, currently function as carbon sinks and are a significant store of carbon within Canada (Timoney, 2003; Kuhry et al., 1993). However, increasing evaporative demand could produce drier conditions resulting in "browning", and the release of stored carbon, functioning as a positive feedback to increasing climatic warming (Gorham, 1991; Vasander and Kettunen, 2006; Turetsky et al., 2011; Moore et al., 2013).

Anthropogenic activities in the WBF and BP, in particular, have resulted in disturbances, ranging from the scale of individual forest patches (i.e. forest cut blocks) to entire landscapes (i.e. open-pit mining in the Athabasca Oil Sands Region (AOSR) (Solondz et al., 2008; Brown et al., 2010). In 2018, oil-sands development alone has been estimated to have disturbed in excess of 901 km^2 (Canadian Oil and Natural Gas Producers, 2018). Such landscape modifications alter energy budgets and turbulent processes that control evaporative losses from these wetlands, and therefore threaten the hydrologic stability of these ecosystems (Alberta Environmental Protection, 1998; Global Forest Watch, 2000; Petrone et al., 2007; Johnson and Miyanishi, 2008; Government of Alberta, 2015; Plach et al., 2016).

Evapotranspiration (ET) is a combination of evaporation (E) from the surface and transpiration (T) from the plants. Within peatlands of the BP, E is often greater than T as peatlands are dominated by non-vascular vegetation such as *Spaghnum* and feather mosses (Johnson et al., 1995) as opposed to vascular vegetation such as sedges *(Juncus balticus, Carex aquatilis*) or trees (*Picea glauca, Betula papyrifer, Larix laricina*). Non-vascular vegetation, such as *Sphagnum* mosses lack the active water transport systems possessed by vascular vegetation (Glime, 2007). Instead, mosses rely on capillary rise and vapor fluxes to draw water from the soil to the moss capitula where growth occurs (Schipperget and Rydin, 1998; Goetz and Price, 2015). However, the rate of vertical movement of water from the soil to the capitulum is highly dependent on the density and porosity of the vegetation mat (McCarter and Price, 2012). Brown et al. (2014) found that if the water table is below the surface, ET is reduced due to the lack of available water for the capitulum. Furthermore, Strack et al. (2009) noted that once the water table is below the surface, its influence on ET is relatively constant until the depth is ≥56 cm below surface. Price (1997) reported a depth of 30 cm below surface, from which the reduced rate of capillary rise from the water table to the surface could be a limiting factor for E (Golubev and Whittington, 2018). Therefore, in non-vascular vegetation surface resistance to E is a function of the vegetation mat density and depth and its resulting aerodynamic resistance, unlike vascular plants where short-term variation in the resistance to E is largely driven by stomatal resistances (Rydin and Jeglum, 2006). Atmospheric moisture demand in a peatland is dominated by non-vascular vegetation, and thus is influenced primarily by moisture availability and available energy (Q^*-Q_g) (where Q^* is net radiation and Q_g is ground heat flux), followed by vapor pressure deficit (VPD) when water is not limiting (Admiral et al., 2006; Brown et al., 2010).

The characteristic mosaic of upland forests and wetlands of the BP produces a landscape characterized by rapid changes in displacement heights that result in flow separation when airflow transitions from taller, forested and shorter, peatland land classes. Leeward of the forest-to-peatland transition the separation of flow produces a region that is sheltered from turbulence, which has been shown to moderate evaporative fluxes throughout the BP (Petrone et al., 2007). Further, large-scale land reclamation projects, such as oil sands mine closure plans in the AOSR, require land leases to be returned back to a functionally equivalent mosiac of upland forests, peat-accumulating wetlands and small surface-water bodies (Daly et al., 2012). Therefore, it is critical to understand the turbulent processes within a heterogeneous landscape as they can influence not only the resilience of natural systems, but also the success of reclamation strategies and constructed ecosystems in the BP.

Numerous studies investigating flow separation over heterogeneous surfaces (Liu et al. 1996; Patton et al. 1998; Belcher et al. 2003; Yang et al. 2006b; Yue et al. 2007; Cassiani et al., 2008; Dupont and Brunet, 2008a; Chatziefstratiou et al., 2014; Markfort et al., 2014) have identified transition structures by using the step analogy where wind either flows into a forward-facing step (FFS) or over a backward-facing step (BFS), with the primary focus being on either the flow approach to or exit from the transition (Detto et al., 2008; Panferov and Sogachev, 2008; Chatziefstratiou et al., 2014). Examination of mean flow over a roughness transition can be conceptualized by combining and modifying the frameworks from Judd et al. (1996) and Cleugh (1998) (Figure 2-1). Based on its turbulent properties, flow leeward of a BFS is classified into several distinct regions:

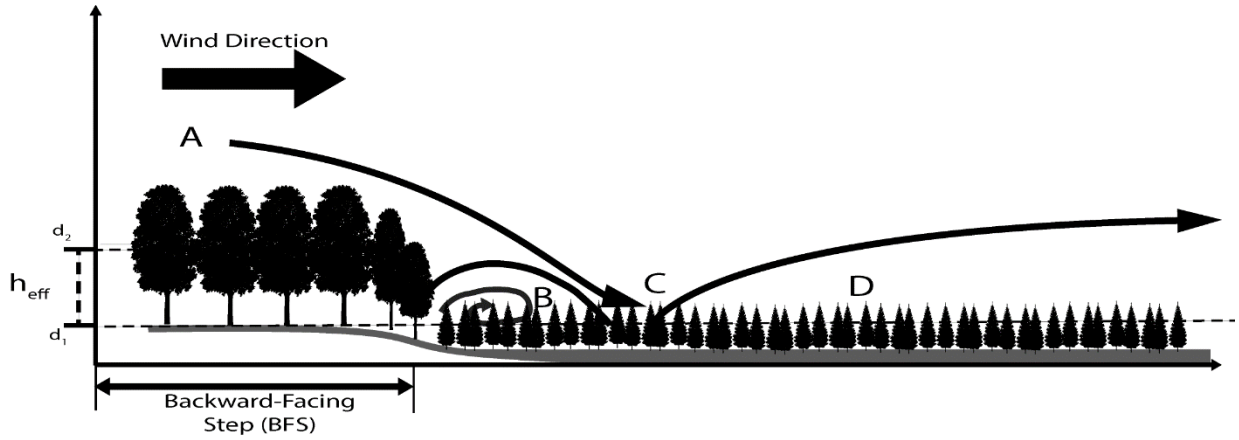

Figure 2-1: Schematic showing the unique zones created by air flow adjusting over a backward-facing step (BFS) transition, illustrating the (A) approach flow; (B) sheltered region; (C) reattachment zone; and (D) recovery region. d_1 and d_2 represent the zero-plane displacement height of the peatland vegetation and upland vegetation, respectively, h_{eff} is the height difference between d_1 and d_2 ($h_{eff} = d_2 - d_1$).

Approach flow (A in Figure 2-1) is characterized as flow that is in equilibrium with the underlying up-step surface roughness elements; such that the flow profile follows the Monin-Obukhov Similarity Theory (MOST) (Monin and Obukhov, 1954). However, the sudden change in displacement height results in a decoupling of the flow profile from the surface, increasing flow velocities and wind shear as flow adjusts to the new down-step surface elements. The decoupling of the flow profile produces a region of reduced streamwise velocities and pressure, which is separate from the mean adjusting layer (B in Figure 2-1). As the mean flow *reattaches* (C in Figure 2-1) with the down-step surface layer, it is characterized as having high flow velocities and turbulent stresses, which produce an adverse pressure gradient at the down-step surface resulting in flow reversals within the *sheltered region* (B in Figure 2-1). The adverse pressure gradient produced is a product of the lower pressures within the sheltered region compared to the higher pressures observed in the reattachment region, which causes flow to oppose the mean flow direction. Flow reattachment distance is influenced by the approach flow turbulence, up-step surface roughness, the state of the boundary layer at the separation point, the geometry of the BFS,

and the height of the BFS transition (Markfort et al., 2014; Van der Kindere and Ganapathisubramani, 2018). Markfort et al. (2014) showed that by increasing turbulence over the BFS the reattachment distance decreased by approximately 50% but increased the distance to equilibrium compared to less turbulent BFS flow. Van der Kindere and Ganapathisubramani (2018) investigated interactions between FFS and BFS blocks, and its impact on flow reattachment leeward of a BFS. They found that when the block lengths were too short to allow for flow reattachment, the reattachment region leeward of the BFS was larger than if the flow had interacted with the surface block before the BFS. Mean flow profile development occurs after the reattachment zone, as flow *recovers* (D in Figure 2-1) and equilibrates with the down-step surface layer roughness. Height of the BFS influences reattachment distance, therefore the distance leeward of the BFS is scaled by using the effective canopy height (h_{eff}), where $h_{eff} = d_2 - d_1$, and d is the zero-plane displacement of the down-step (indicated with $_1$, and in our study, peatland) and the up-step ($_2$, forest) surfaces. Due to the complexites of the flow produced by displacement transitions, single point eddy-covariance (EC) measurements conducted within the area affected by the transition are difficult to interpret and theoretically fail as the assumptions of a homgenous surface layer, zero mean vertial flow, and no vertical divergence of fluxes are not met (Yang et al., 2006a; Lee, 2000; Paw et al., 2000). Therefore, 3-D computational fluid dynamic models that can resolve turbulence at the forest-to-peatland transition must be employed to generate a better understanding of flow dynamics within such environments (Bohrer et al., 2009).

In this study, I used the Regional Atmospheric Modelling System (RAMS)-based Forest Large Eddy Simulation (RAFLES) (Bohrer et al. 2009) to assess the sensitivity of evaporative demand to turbulence over a BFS representing the transition from forest to peatland. The primary objectives of this study are to: 1) show the differences in flow properties leeward of a BFS

transition; 2) quantify the influence of surface roughness on flow around a BFS transition; and 3) estimate the implications of BFS transitions and canopy roughness on evaporative fluxes.

2.2.0 Materials and Methods

2.2.1 Site Description

This modelling experiment utilized synthetic landscapes, based on a mix of real vegetation/land classes and characteristics from multiple regions within the BP, including the AOSR, to examine the influence of displacement and roughness transitions on turbulent flow.

Meteorological data used to set up the site parameters that were prescribed for the upland-forest land classification components of the simulations (Table 2-1) were obtained from Pond 40 (56° 4'21.90" N, 115°28'33.30" W) in the Utikuma Region Study Area (URSA) near Utikuma Lake, northern Alberta. This site is dominated by dense, mature aspen (*Populus balsumifera* and *Populus tremuloides*), with mean canopy height of 25 m and summer time mean LAI of 2.83 m^2/m^2. It is located on gently sloped hills adjacent to low lying wetlands. The mean growing season temperature at this site is 13.4 ^oC, it is a dry site with ET: PET (Priestly-Taylor) ratio of 0.67. The EC system used to parameterize the upland was installed on a tower at 23.5 m above the forest canopy, to yield a footprint area large enough to encompass landscape-scale variability (Brown et al. 2010, 2013; Devito et al., 2005; Petrone et al., 2015; Sutherland et al., 2017).

The meteorological data used to set up the site parameters that were prescribed for the low-roughness peatlands represented in the model (Table 2-1) were obtained from a constructed fen-peatland/upland complex ~20 km north of Fort McMurray Alberta, Canada (56° 55.944′ N, 111° 25.035′ W). The EC flux tower site is located at a constructed fen-peatland/upland complex with a vegetation cover comprising of saline (*Juncus balticus*, *Calamagrostis inexpansa*, *Triglochin martima*) and freshwater (*Carex aquatilis*, *Betula glandulosa*) peatland plant species (Nwaishi et

al., 2016) with a mean vegetation height of 1.25 m and a mean summer time LAI of 2.45 m^2/m^2. The mean growing season temperature at this site is 12.8 ^oC; it is a wet site with ET: PET (Priestly-Taylor) ratio of 1.03 with the EC sensors measuring at a height of 2.5 m. Additional site details can be found in Ketcheson et al. (2017) and Nwaishi et al. (2016).

Site parameters describing a medium-roughness wetland were prescribed based on observations at Poplar fen, which is located ~20km north of Fort McMurray Alberta, Canada (56°56′ N, 111°932′ W). Poplar fen is a nutrient-rich, densely forested peatland dominated by *Larix laricina*. This site is characterized as being a large, shallow gradient peatland surrounded by low relief riparian and mixed wood uplands (*Populus tremuloides, Pinus banksiana, Picea mariana*) with a mean vegetation height of 6.47 m and a mean summer time LAI of 1.33 m^2/m^2. The mean growing season temperature at this site is 13.8 ^oC; it is a wet site with ET: PET (Priestly-Taylor) ratio of 0.9, with the EC sensors measuring at a height of 7.5 m. More details on this study site can be found in Elmes et al. (2018). Meteorological and vegetation data were both collected from the same location and are summarized in Table 2-1.

Finally, the high-roughness peatland was prescribed based on observations from an undisturbed moderate-to-rich peatland site, Super 8 (56° 4'48.80" N, 115°31'57.06" W), located in the Utikuma Region Study Area (URSA) near Utikuma Lake, northern Alberta. Super 8 is dominated by sparse *Picea glauca* along the north side and *Betula papyrifer* along the south end of the fen, underlain by Sphagnum mosses. For this study, the *Picea glauca* was used as the vegetation analogue for the roughness parameterization with a mean vegetation height of 3.56 m and a mean summer time LAI of 1.75 m^2/m^2. The mean growing season temperature at this site is 12.6 ^oC; it is a relatively dry peatland compared to the other peatlands within this study with an ET: PET (Priestly-Taylor) ratio of 0.75 observed from an EC system measuring at a height of 6.5

m. The peatland is surrounded by a ~25 m sloping forest canopy dominated by (*Populus balsumifera* and *Populus tremuloides*) that exhibit a sharp transition from peatland to upland (Table 2-1).

EC measurements for the upland forest and low roughness peatland locations were collected using a LI-7500 (LI-COR: Lincoln, Nebraska, USA) open path IRGA paired with a CSAT3 3D sonic anemometer (Campbell Scientific: Logan, Utah, USA) at a height of 23 m and 3 m scanning at 20 Hz during the years of 2008 and 2015, respectively. EC measurements in the medium and rough peatlands were collected using an LI-7200 (LI-COR: Lincoln, Nebraska, USA) closed path IRGA and Windmaster Pro sonic anemometer (Gill Instruments: Lymington, UK) at a height of 6 m, scanning at 20 Hz during 2015. All flux data were processed into 30-minute average fluxes using, and filtered for periods of low atmospheric turbulence (u_*), corrected for density and sensor separation (Webb et al., 1980; Leuning and Judd, 1996; Petrone et al., 2015) and flux footprint (Kljun et al., 2004). Final corrections and gap-filling followed the methods outlined in Petrone et al. (2001), Wilson et al. (2002) and Brown et al. (2010). Net radiation was measured at all sites using a NR-Lite2 (Kipp & Zonen; Delft, Netherlands) at the same height as the EC measurements. Ground heat flux was calculated using ground heat flux probes (HFT3; Campbell Scientific: Logan, Utah, USA) and ground temperature profiles at all sites (Halliwell and Rouse, 1987; Petrone et al., 2000; Petrone et al., 2006).

Stand density, canopy height and trunk taper functions were determined by averaging three random 10 m × 10 m sampling plots (Table 2-1) at each site. To remove understory and smaller vegetation that was negligible for the simulation, trees with a circumference at breast height that were less than 5 cm were ignored. Taper functions were produced by creating a logarithmic regression between diameter at breast height and the height of the vegetation following Naidu et

al. (1998). LAI at the low- and medium-roughness scenarios was measured using an LP-80 LAI probe (Decagon Devices, Washington, USA) during peak growing season at 9 points within each of the vegetation survey plots. LAI collected in the upland forest was collected using LP-80 LAI probe during peak growing season at points along a transect that captured site variability. LAI measurements in the high roughness peatland were sampled using an LAI-2200C plant canopy analyzer (LI-COR: Lincoln, Nebraska, USA) during peak growing season with observation points following a transect throughout the site to determine the spatial variation and autocorrelation length of LAI. Leaf area density (LAD) profiles were created by falling 2 - 3 trees per land class and measuring the height, trunk diameter and crown diameter at 1m vertical intervals. To obtain a crown volume, I assumed a uniform circular diameter of the canopy at each height interval, with all leaves stripped and sorted into 1m intervals. For coniferous vegetation, every other 1 m section was used and interpolated between the heights due to the difficulty with transportation and removing needles. All vegetation was dried to standardize weight, and a 10 g sub-section was selected and measured using LI-3100C leaf-area meter (LI-COR: Lincoln, Nebraska, USA) using a resolution of 0.1 mm^2. The area of the 10 g was then used to scale-up the remainder of the sample and applied to the volume of the crown.

2.2.2 Simulation setup

RAFLES was used to resolve flow inside and above heterogeneous, three-dimensional (3-D), forest canopies by solving the 3-D Navier-Stokes equations for a rectangular grid (Bohrer et al. 2009). The canopy representation in RAFLES includes a multi-layer, 3-D heterogeneous canopy, where each canopy-containing voxel is prescribed with volume and aperture restriction to the flow due to the presence of modeled trees, and leaf density that exerts drag on the flow and acts as a source of heat and water vapor fluxes (Bohrer et al. 2009). Volume and aperture restrictions

interact with the numerical solution of the flow following the shaved grid-cell method (Adcroft et al., 1997, Bohrer et al. 2009).

The simulation domain used in this study was set to 1000 × 1000 × 1040 m^3, yielding 250 × 250 × 107 (x, y, z) Cartesian grid points, with a horizontal grid resolution of 4 × 4 m^2, and vertical grid resolution of 2 m (from the ground, to a height of 100 m). Above 100 m, a 10 % vertical stretching was applied for each consecutive vertical layer to a maximum vertical grid height of 25 m. Each 3-hour simulation included a spin up period lasting 2.5 hours with the observational period consisting of the last 30 minutes. The model timestep was 0.05 seconds, with an output of a full domain snapshot every 2 seconds, for a total of 900 output files averaged into 30-minute flux period. The 30-minute mean flux was compared with eddy covariance (EC) flux measurements (described below). Further details of RAFLES' formulation and numerical schemes can be found in Bohrer et al. (2009).

2.2.3 Virtual canopy setup

The V-CaGe model was used to translate 2-D images of leaf area density and information about canopy height, height variability and vertical leaf area density profiles into detailed, 3-D fields of numerical canopy elements for each type of land cover (Bohrer et al., 2007, Chatziefstratiou et al. 2014). V-CaGe was used to generate a virtual simulation domain with different land-cover patches, consistent with the observed canopy characteristics, and with the mean surface roughness classes. The domain consisted of one rectangular forest block followed by three rectangular blocks that represent the three potential peatland roughness classes classified as smooth, medium, and rough (Figure 2-2A, B).

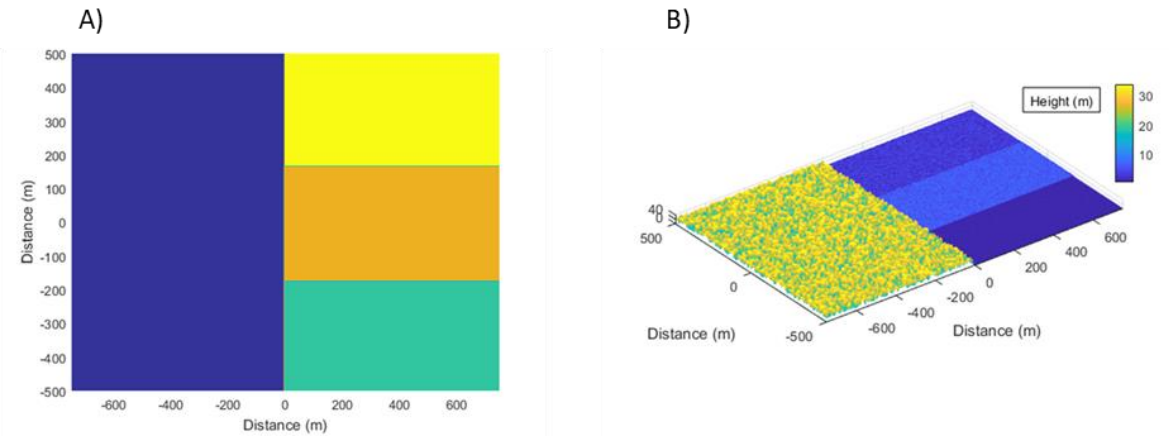

Figure 2-2: A) representation of the patch type of the simulation, with purple representing the upland forest and yellow (high); orange (medium); and teal (low) peatland roughness's; B) illustrates the canopy heights associated with the patch types shown in A.

Within each patch type, 3-D heterogeneous random canopy features (leaf area density, aperture and volume restriction in each canopy containing voxel) were generated such that the patch statistics are consistent with the mean and variability of leaf area index, canopy height, stem diameter and stand density of the observed ecosystems these patch types represent in the virtual experiment. V-CaGe further upscales the prescribed mean sensible and latent heat fluxes and surface albedo for each patch type to each model voxel proportional to the leaf area index of the canopy column and light attenuation throughout the column (Table 2-1). The prescribed fluxes were based on observed Bowen ratio (H/LE) and the sum of turbulent fluxes ($H + LE$), and were measured using one eddy covariance tower within each patch type at the sites described above, where H and LE are the sensible and latent heat flux, respectively during the summers of 2008 and 2015. To standardize the data among sites, the average of daytime (10:00-17:00) conditions during the growing season (Day of year (DOY) 152 - 243) were used to prescribe the fluxes within each patch type.

Table 2-1: Values used for patch type parameterization in V-CaGe. [1] Values are taken from Betts et al. (1997) (Table 2). [2] Values taken from Thompson et al. (2015). Where the upland forest is Pond 40; low roughness is the constructed fen; medium roughness Poplar; and the high roughness is Super 8.

Canopy parameters	Forest Upland	Low Roughness	Medium Roughness	High Roughness
Stand density (stems/ha)	2600	10000	5150	2700
Mean canopy height (m)	25	1.25	6.47	3.56
Std of canopy height	8.9	0.25	2	1.5
Mean LAI (m^2/m^2)	2.83	2.45	1.33	1.75
Std of LAI	1.38	1.45	0.76	0.61
Mean Bowen ratio	1.1	0.44	0.68	0.81
Std of Bowen ratio	0.65	0.25	0.33	0.73
Mean canopy-top total flux forcing (W/m^2)	323.84	401.56	364.06	397.5
Std of canopy-top total flux	118.89	21.23	218.55	221.28
Mean Albedo	0.16 [2]	0.13	0.11 [1]	12
STD Albedo	0.01 [2]	0.18	0.02 [1]	0.3

2.2.4 Initial conditions and forcing

The RAFLES simulation was initialized using horizontally homogeneous and vertically prescribed profiles of horizontal wind, humidity, and temperature. For the purpose of initialization, wind profiles were prescribed using the Monin-Obukhov similarity (Monin and Obukhov, 1954).

$$\overline{u_z} = \frac{u^*}{\kappa}\left[ln\left(\frac{z-d}{z_0}\right) - \psi_m\left(\frac{z-d}{L}\right) + \psi_m\left(\frac{z_0}{L}\right)\right] \quad (1)$$

where $\overline{u_z}$ is the mean streamwise wind velocity at height z above the ground, u_* is the frictional velocity, κ is the von Kármán constant (0.41), d is the displacement height estimated as $d \approx 2/3h$ (where h is the mean canopy height), Z_0 is the roughness length estimated as $Z_0 \approx 0.1h$. ψ_m was used a correction term to account for convective boundary layer conditions following Paulson (1970):

$$\psi_m(x) = 2ln\left[\frac{1+(1-16x)^{\frac{1}{4}}}{2}\right] + ln\left[\frac{1+(1-16x)^{\frac{1}{2}}}{2}\right] - 2\,tan^{-1}\left[(1-16x)^{\frac{1}{4}}\right] + \frac{\pi}{2} \quad (2)$$

where x is either $(z - d)/L$, or Z_0/L.

Equation 1 was prescribed based on observed conditions at the upland EC tower where h = 25 m, u_* = 0.53 ms^{-1}, L = -124.11 m were derived using the same criteria for V-CaGe surface fluxes selection. Vertical profiles of potential temperature and water vapor mixing ratio were prescribed using observed data from Fort Smith, Alberta (YSM) atmospheric sounding station (data obtained from the University of Wyoming database: http://weather.uwyo.edu/upperair/sounding.html) on August 31st, 2015 at 12:00 PM. All forcings were interpolated linearly to 25 m intervals to fit the vertical forcing prescription of RAFLES. Temperature, and humidity profiles, and turbulent wind fields were allowed to evolve after initialization during the simulation. Forcing included the surface fluxes that are prescribed throughout the simulation from each soil surface and vegetation-containing voxel following a spatial distribution as explained above, and a lateral wind nudging to maintain the prescribed mean vertical wind profile aloft (above a height of 4h). This is equivalent of prescribing a geostrophic wind gradient, but does not require a priori knowledge of the total surface drag force to balance the geostrophic wind.

2.2.5 Analysis of simulation results

The canopy aerodynamic resistance to moisture transfer was calculated through the moisture diffusion equation:

$$r_q = -Lv\rho\left(\frac{q_a - q_c}{LE}\right) \quad (3)$$

where r_q is the canopy aerodynamic resistance to moisture transfer, Lv is the latent heat of vaporization of water, ρ is air density, q_a is the water vapor mixing ratio at height above the canopy, q_c is the canopy-air water vapor mixing ratio, and LE is the net surface + canopy latent heat flux.

2.3.0 Results

2.3.1 Spatial structure of wind speed

Within the sheltered region of the medium and high roughness scenarios, surface streamwise wind velocities continually accelerate until an equilibrium of $\bar{U}_h/\bar{U}_0$ = 0.65 and 0.75 was achieved at $x/h_{eff} \approx$ 25 and 15 (Figure 2-4A), for the medium and high roughness, respectively. $\bar{U}_h$ is the streamwise velocity at the top of the peatland vegetation, where *h* denotes the upwind forest canopy height, and $\bar{U}_0$ is a reference streamwise velocity measured at *z/h*=2 of the upland forest canopy. At $x/h_{eff} \approx 2$, within the low roughness scenario (Figure 2-4A), peak flow reversal occurs with respect to the streamwise velocity with a velocity of $\bar{U}_h/\bar{U}_0$ = -0.15. Following $x/h_{eff} > 2$ within the low roughness scenario, streamwise velocities steadily recovered until equilibrium flow rates occur at $x/h_{ef} \approx 20$, where $\bar{U}_h/\bar{U}_0 \approx 0.6$. No relationships were observed between the rate of flow acceleration in the reattachment region and canopy roughness. However, increasing surface roughness does increase the sharpness of the transition between flow acceleration and flow equilibrium.

In all cases, persistent upward flow $\bar{w}_h \approx 0.2$ ms^{-1} occurred near the transition $x/h_{eff} < 1$ followed by a shift to maximum downward velocities between $x/h_{eff} = 3 – 4$ which indicates that the flow is interacting with the peatland surface (Figure 2-3, 2-4B). Following the maximum downward velocities, vertical wind speeds transition towards an equilibrium where $\bar{w}_h \approx 0$ m/s at $x/h_{eff} \approx 15$.

2.3.2 BFS Effects on Turbulent Flow

Across the BFS flow transition, mean turbulent intensity, indicated by the standard deviation of the vertical wind velocity, $\sigma(w)$, is lowest in the low roughness cases and increases with surface roughness (Figure 2-5A). Variability of observed $\sigma(w)$ across the BFS transition also increases with increasing surface roughness. For all roughness cases, maximum $\sigma(w)$ of 0.041, 0.122, 0.189

m/s occurs between x/h_{eff} = 2-3 and decreases with distance to the surface equilibrium rate of 0.008, 0.037, 0.080 m/s at x/h_{eff} ≈17, 16, 15 for the low, medium and high roughness respectively.

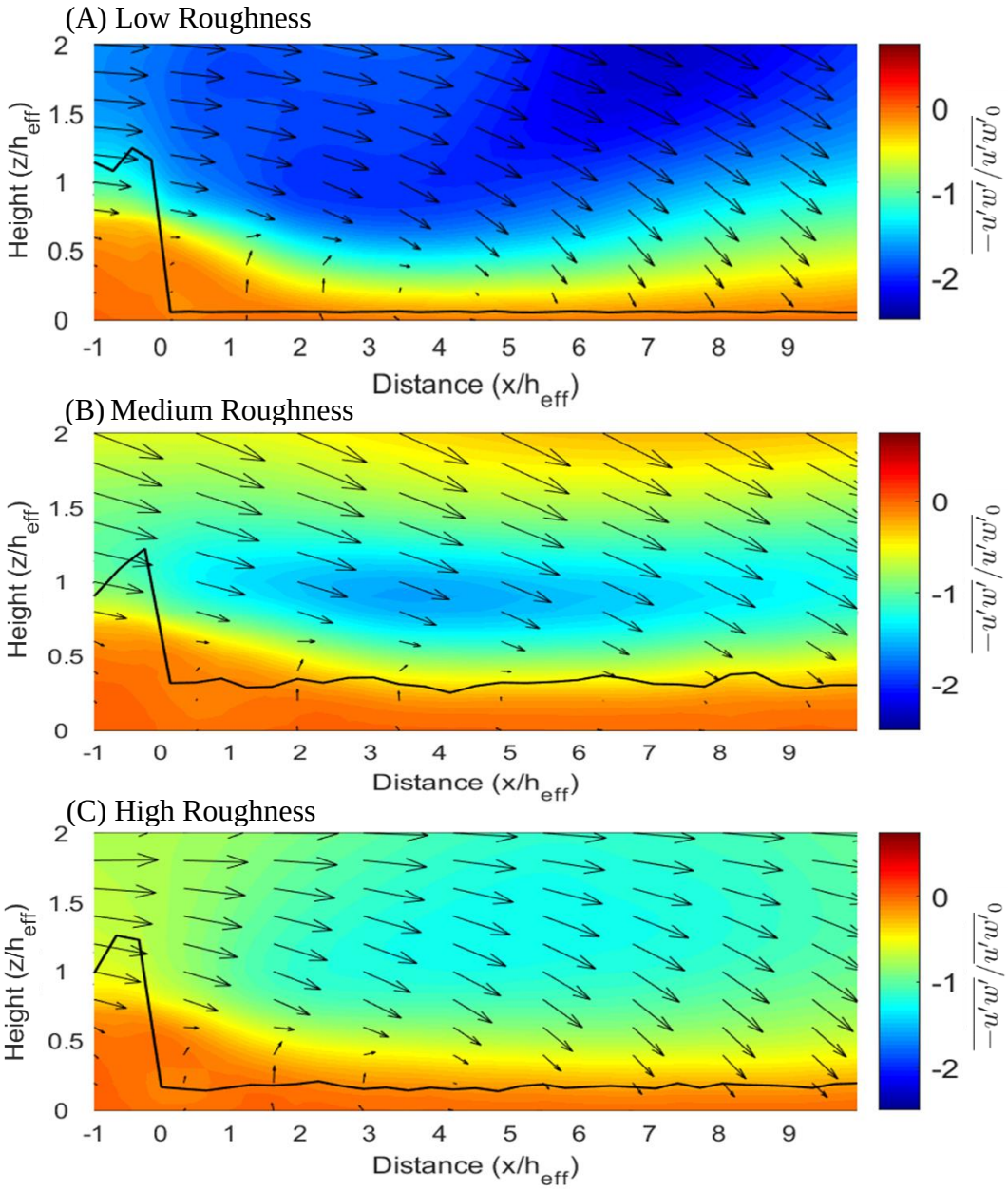

Figure 2-3: Cross section of mean streamwise wind velocity ($\bar{u}$) [ms^{-1}] normalized by the mean windspeed at twice the upland canopy top height, $z/h_{eff}=2$, where arrows mark the wind velocity along the streamwise and vertical components. The x-axis marks the downwind horizontal distance from the BFS transition relative to h. The z-axis marks the vertical elevation above ground relative to h_{eff}. Solid black line in each panel denotes the forest canopy top. Color map marks the Reynolds Stress normalized by the Reynolds Stress at reference height, z/h=2. Panel (A) shows the results for a low roughness patch, (B) the medium roughness patch and (C) the high roughness patch.

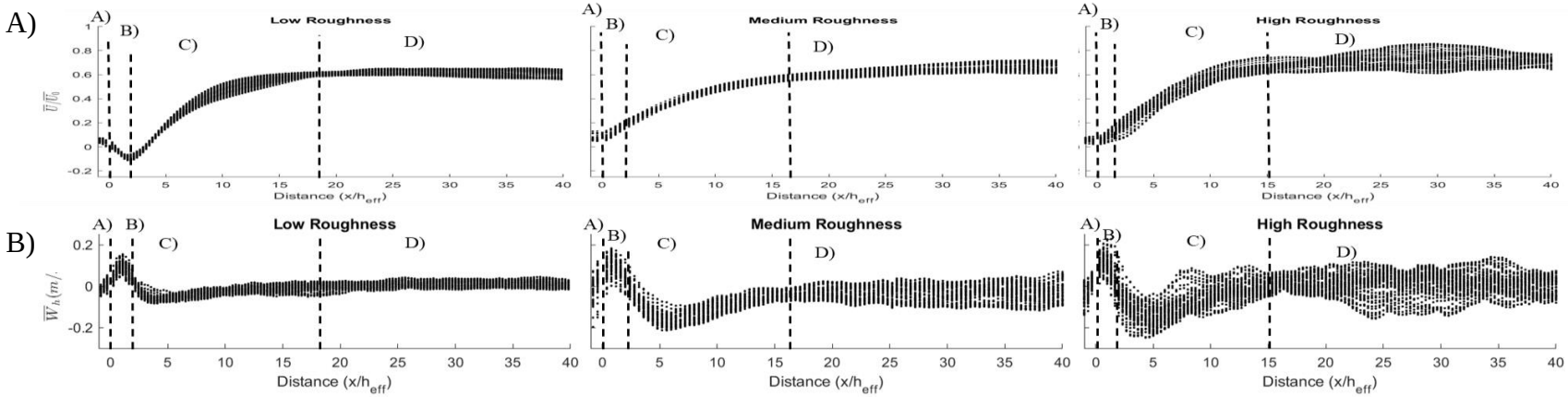

Figure 2-4: A) Mean streamwise velocities ($\overline{U}$) [ms^{-1}] measures at height h across low, medium and high roughness cases (left to right) with the x-axis being the distance from the BFS transition relative to the mean canopy height of the upland forest. B) Mean vertical windspeed ($\overline{w}$) [ms^{-1}] measures at height h across low, medium and high roughness cases (left to right) with the x-axis being the distance from the BFS transition relative to the mean canopy height of the upland forest. Dotted lines within each figure represent flow regions where A) is the flow within the forest (x/h_{eff} = -1 to 0); B) sheltered region; C) Reattachment region; D) Recovery Region.

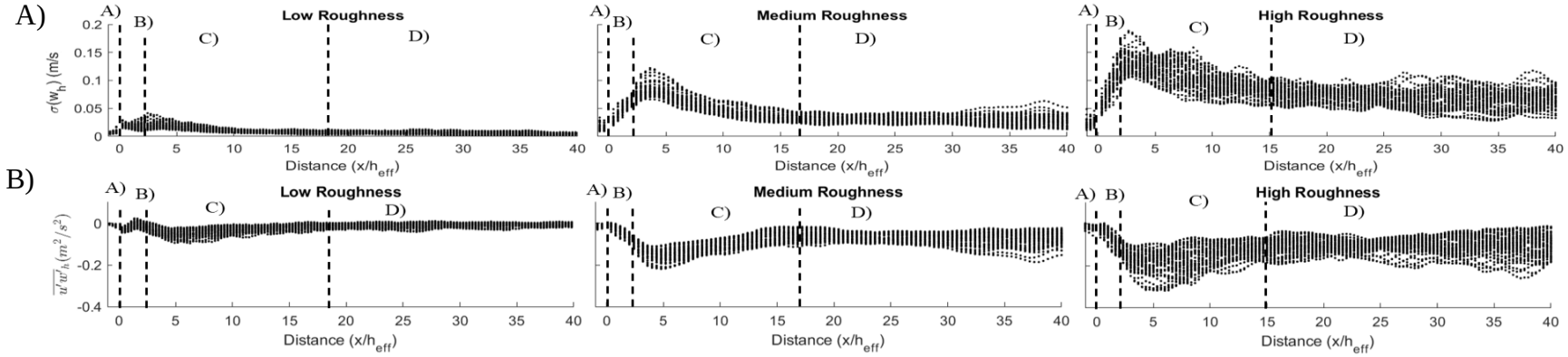

Figure 2-5: A) Turbulent intensity (σ(w)) [ms^{-1}] measured at height h within the peatlands across low, medium and high roughness cases (left to right) with the x-axis being the distance from the BFS transition relative to the mean canopy height of the upland forest. B) Kinematic Reynolds stress ($\overline{u'w'}$) [m^2s^{-2}] measured at height h within the peatlands across low, medium and high roughness cases (left to right) with the x-axis being the distance from the BFS transition relative to the mean canopy height of the upland forest. Dotted lines within each figure represent flow regions where A) is the flow within the forest (x/h_{eff} = -1 to 0); B) sheltered region; C) Reattachment region; D) Recovery Region.

Within all roughness cases, the sheltered region is separated from the reattaching flow by a sharp gradient of turbulent stress (Figure 2-3). Within the medium and high surface-roughness scenarios are $\overline{u'w'} \approx 0$ m^2s^{-2} at $x/h_{eff} = 0$ (Figure 2-5B). Between $x/h_{eff} = 3$ - 5 Reynolds stress reached its minimum where $\overline{u'w'}$ = -0.15 and -0.24 m^2s^{-2} for the medium and high roughness, respectively. Reynolds stress responds differently within the low roughness scenario where $\overline{u'w'}$ ≈ -0.05 m^2s^{-2} at $x/h_{eff} = 0$ and increases to 0.023 m^2s^{-2} at $x/h_{eff} = 1 – 2$. Subsequently, Reynolds stress drops to its minimum of -0.1 m^2s^{-2} between $x/h_{eff} = 5$ - 7 followed by its rebound to an equilibrium at $x/h_{eff} \approx 17$. As surface roughness increased, the magnitude and variability of Reynolds stress increased as well, with values of -0.016 ± 0.017, -0.054 ± 0.025 and -0.084 ± 0.034 m^2s^{-2} being observed within the low, medium and high surface roughness cases, respectively. As surface roughness increases, Reynolds stress's experience a sharper transition to equilibrium rates that occur at $x/h_{eff} \approx 16$, 15 for the medium and high surface roughness cases respectively.

2.3.3 Canopy resistance to moisture transfer

In all cases, streamwise turbulent intensity, σ(u), is greatest at the forest canopy height, z/h=1, and shortly downwind of the transition, between x/h_{eff} = 1-3 (Figure 2-6A). By x/h_{eff} = 8 σ(u) has adjusted to the peatland surface as indicated by the adjusted flow profile. However, for the low roughness scenario, the flow profile does not fully develop until $x/h_{eff} > 30$ which is in line with Markfort et al. (2014) for smooth surfaces. For all cases, water vapor mixing ratio becomes well-mixed (loses its vertical gradient) at the height of about z/h_{eff} =2 (Figure 2-6B). A greater difference between mixing ratio aloft (q_{air} at z/h=4) and near the surface (q_h at z/h=1) is observed in the low roughness scenario, which corresponds with the higher moisture conditions at the surface due to the higher latent heat flux that is characteristic of the ecosystem type this surface represents.

In all scenarios, the highest surface resistance to moisture transfer (r_q) happens shortly downwind of the transition, at x/h_{eff} = 1 (Figure 2-6C). While in the reattachment zone, between x/h_{eff} = 3-8 r_q is at its lowest rates as turbulent interactions with the canopy are the highest. Beyond x/h_{eff} > 8 in the flow recovery region, r_q begins to increase as flow recovery occurs and a developed boundary begins to form to the roughness elements of the peatland surface. Vertically integrated mean r_q rates, defined as the resistance to moisture transfer between the surface (q_h) and the well-mixed atmosphere (q_{Air} measured at z/h_{eff} =2) is the highest in the low roughness scenario 11.31 ± 1.73 s/m followed by 9.46 ± 1.28, and 8.03 ± 1.27 s/m for the medium and high roughness scenarios respectively (Figure 2-7). r_q rates the recovery region of the low roughness scenario steadily increase an equilibrium is achieved at x/h_{eff} = 35 and approximately x/h_{eff} = 20 and x/h_{eff} = 25 in the medium and high roughness scenarios respectively (Figure 2-8B).

For all cases, heat and water vapor accumulation occurs at the BFS transition (x/h_{eff} = 0) (Figure 2-8A, 2-B) where K_h is approximately 1.5 K^o greater than outside of the sheltered zone. Downwind from the transition, between x/h_{eff} = 5 - 7, temperatures and water vapor transition to the equilibrium values. Temperatures are higher and more variable in the lower roughness scenarios as opposed to the higher roughness scenarios with mean temperatures of 296.4 ± 0.22, 295.6 ± 0.18, 295.8 ± 0.16 K^o for the low, medium, and high roughness scenarios respectively (Figure 2-8A). Water vapor mixing ratio is similar to the temperature dynamics of the BFS in that the lower roughness surfaces have higher mean values and variability. However, water vapor concentrations between flow regions have greater differences in the low roughness case when compared to the medium and high roughness cases (Figure 2-8B).

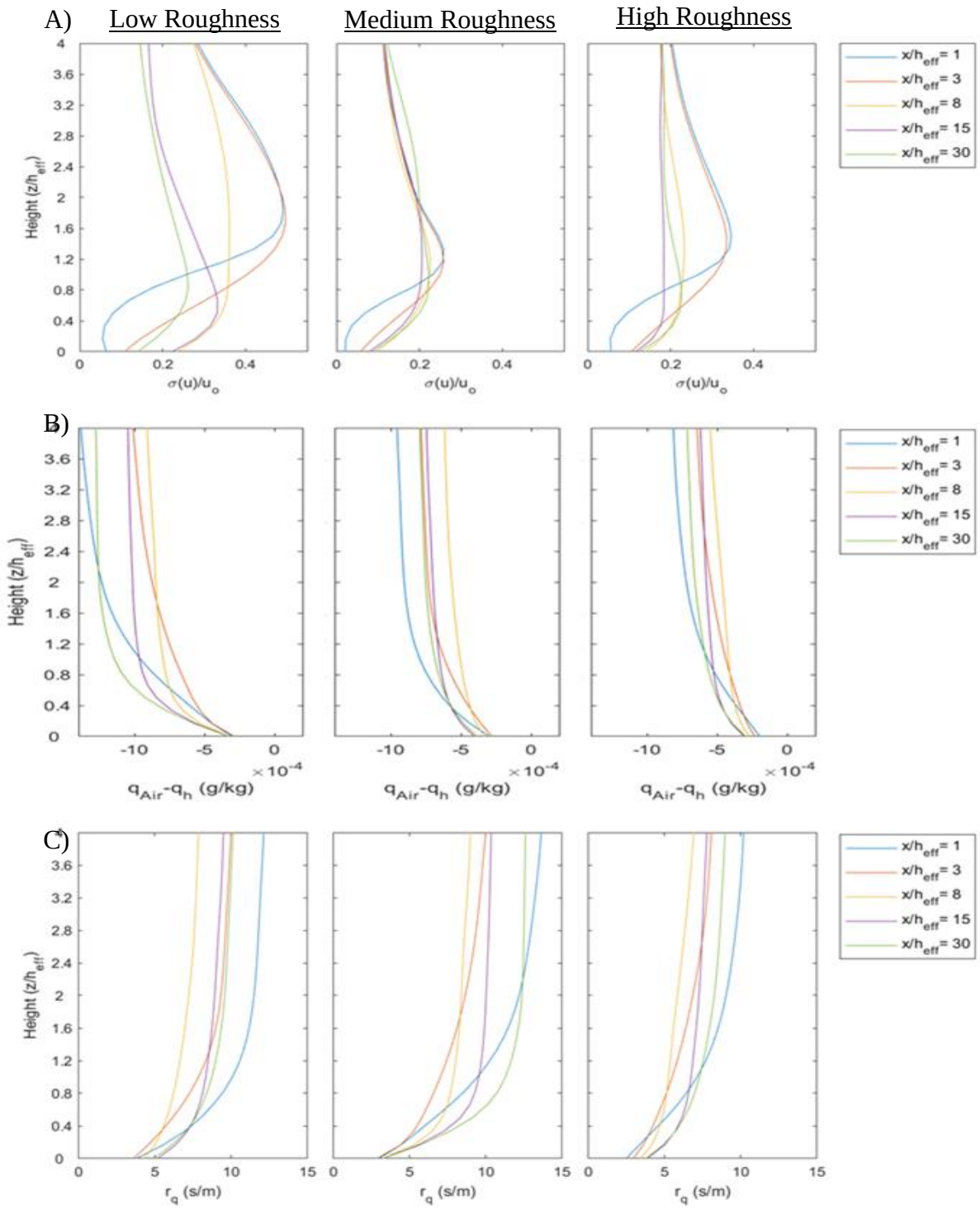

Figure 2-6: A) Vertical profiles of the streamwise turbulent intensity normalized by the mean streamwise velocity at z/h_{eff} =2 ($\sigma(u)/u_o$) where each line represents a distance leeward of the BFS where plots from left to right are low, medium and high roughness. B) Vertical profiles of the mixing ratio gradient from the surface to z/h_{eff} =4 (q_{Air}-q_h) [g/kg] where each line represents a distance leeward of the BFS where plots from left to right are low, medium and high roughness. C) Vertical profiles of the surface resistance to moisture transfer (r_q) [s/m] where each line represents a distance leeward of the BFS where plots from left to right are low, medium and high roughness.

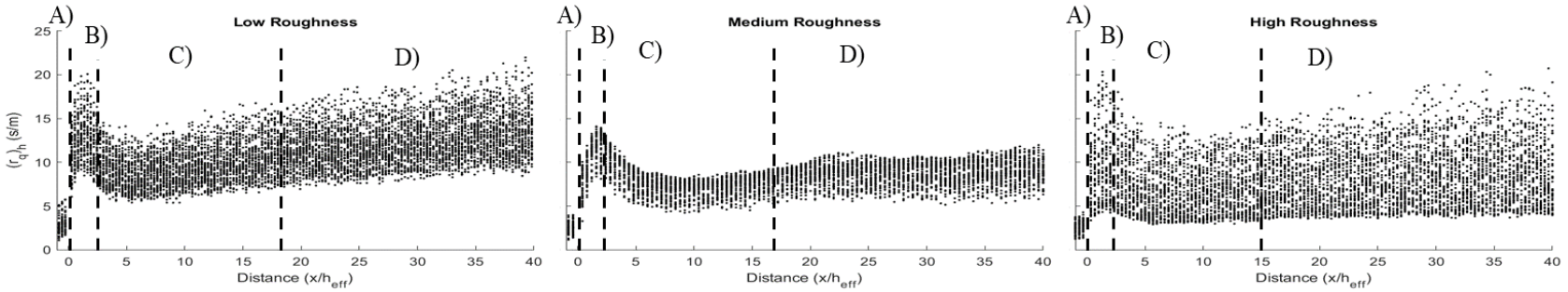

Figure 2-7: Canopy resistance to moisture transfer (sm^{-1}) measured at height h within the peatlands across low, medium and high roughness cases (left to right) with the x-axis being the distance from the BFS transition relative to the mean canopy height of the upland forest. Dotted lines within each figure represent flow regions where A) is the flow within the forest (x/h_{eff} = -1 to 0); B) sheltered region; C) Reattachment region; D) Recovery Region.

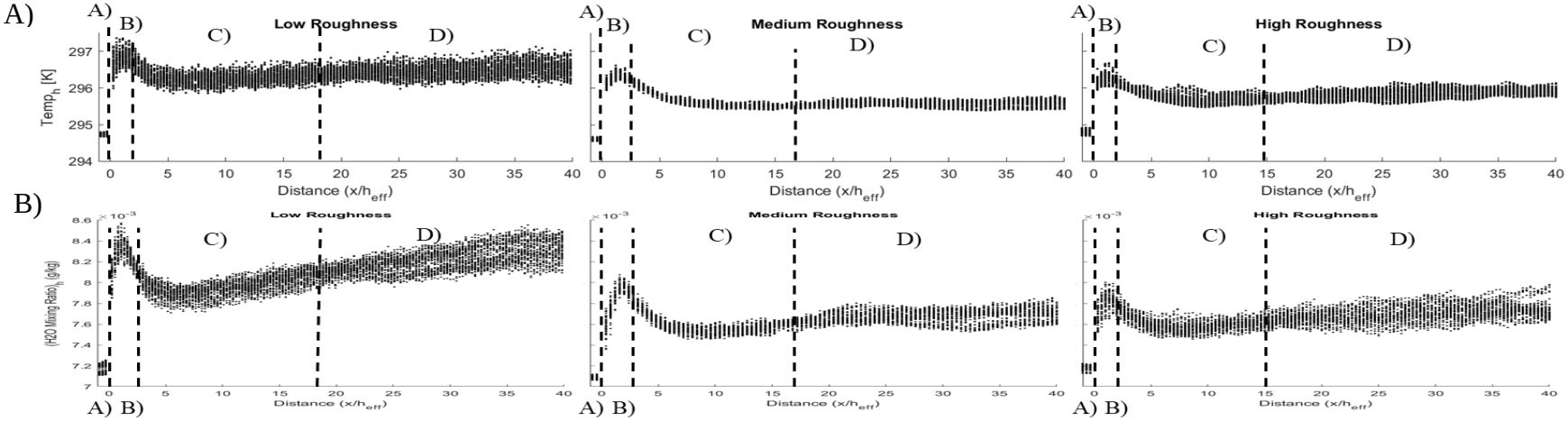

Figure 2-8: A) Temperature [K] measured at height h within the peatlands across low, medium and high roughness cases (left to right) with the x-axis being the distance from the BFS transition relative to the mean canopy height of the upland forest. B) Water vapor mixing ratio [g/kg] measured at height h within the peatlands across low, medium and high roughness cases (left to right) with the x-axis being the distance from the BFS transition relative to the mean canopy height of the upland forest. Dotted lines within each figure represent flow regions where A) is the flow within the forest (x/h_{eff} = -1 to 0); B) sheltered region; C) Reattachment region; D) Recovery Region.

2.4.0 Discussion

2.4.1 Micrometeorological Interactions

The sheltered region within all simulations occurs between $x/h_{eff} = 0 - 2$ downwind of the BFS and is characterized by having low streamwise wind velocities and turbulence that lead to higher water vapor mixing ratios and temperatures. Between $x/h_{eff} = 2 - 3$ leeward of the BFS, $\sigma(w)$ peaks as the mean flow begins to interact with the peatland surface, indicated by downward velocities, decreased water vapor mixing ratios and temperatures and increasing streamwise wind velocities (Cleugh, 1998). Flow recovery begins by $x/h_{eff} \approx 15$ as streamwise wind velocities reach an equilibrium, and $\sigma(w)$ and Reynolds stresses have largely adjusted to the surface, with minor adjustments occurring at distances greater than $x/h_{eff} = 25$. These characteristics define the boundaries between the turbulent regions that control scalar fluxes and are within the range of lengths in theoretical, observed and modeled studies (Cleugh, 1998; McNaughtan, 1988; Wang and Takle, 1997; Yang et al., 2006b; Markfort et al., 2014).

Peatland canopy roughness does not influence the flow-reattachment distance, as it is primarily driven by upwind factors, such as the geometry of the BFS, state of the boundary layer at the separation point, freestream turbulence, and upwind surface roughness (Markfort et al., 2014; Kindere and Ganapathisubramani, 2018). However, within the peatland, a faster and sharp transition of Reynolds stress and streamwise wind velocities to equilibrium rates shows that the rougher scenarios recover faster than the lower roughness scenarios as a result of the more efficient momentum flux that occurs over rougher surfaces (Raupach et al., 1996; Finnigan, 2000; Aubinet et al., 2012).

2.4.2 Impact of BFS and surface roughness on hydroclimatic fluxes

Across all roughness cases, r_q was highest in the sheltered region as there is reduced turbulence (Figure 2-7) resulting in less scalar transfer from the surface to the atmosphere from this region as evidenced by the high temperatures and vapor concentrations (Figure 2-8A; 2-8B). While in the reattachment region higher turbulence results in low r_q rates and the largest drop in temperature and vapor concentrations which suggests that greater surface moisture transfer and therefore evaporative demand will occur in this region compared to the sheltered or the recovery region. After flow reattachment, flow recovery begins as surface turbulence subsides and reaches an equilibrium with the surface, which can either stabilize or increase r_q as the development of the new boundary layer allows for fluxes to reach equilibrium between the atmospheric demand and the surface supply (Vogel and Eaton, 1985; Petrone et al., 2007). r_q stabilizes in the recovery region for the medium and high roughness cases (Figure 2-7B; 2-7C) as the flow profile is suffienctly mixed and atmospheric demand and the surface supply of moisture are in an equilibrium. However, in the low roughness scenario r_q increases in the recovery region as a result of the higher moisture flux from this surface, combined with the decreased turbulence and therefore turbulent mixing, which increases the moisture gradient between the surface to atmosphere and the resistance of the surface to moisture transfer. This increase in r_q stabilizes once the vapor concnetrations at the surface stabilize since the surface supply of moisture are in an equilibrium.

Microclimates produced by the BFS influence the interactions between the vegetation and air as this interaction is strongly correlated to meteorological conditions such as temperature, VPD, light and moisture availability (Davis and Norman, 1988; Oke, 1988; Irmak and Mutiibwa, 2010). The response of the vegetation to the microclimatic conditions is dependent on the moisture

availability at the surface, the moisture demand of the atmosphere and the composition of vegetation (non-vascular, vascular, canopy coverage) which adds more complexity when assessing the evaporative response of the vegetation to microclimatic conditions. For example, Pepin et al. (2002) found that the stomata of black spruce in a peatland experienced a greater stomatal response to an increasing VPD during a dry year as opposed to a wet year; showing that when moisture is available, mass exchanges occur more freely as opposed to when water is limited. In contrast nonvascular vegetation lack stomatal controls, meaning that if moisture is available and there is an atmospheric demand for that moisture, E will occur. However, if moisture is limited, E will be limited by the rate of capillary rise (Strack et al., 2009). Typically, peatlands of the BP experience high water tables and moisture conditions early in the growing season after ice melt, which increases ET rates until the surface begins to dry later in the growing season (Goodine et al., 2008) producing seasonal variability in the response of vegetation to microclimates.

The addition of canopy coverage upwind of the peatland surface will reduce E rates by sheltering the surface vegetation from solar radiation and turbulent transport processes (Brown et al., 2014; Kettridge et al., 2013) depending on the roughness of the surface and stand density of the canopy (Molder and Kellner, 2002; Niu and Yang, 2004). Nevertheless, the addition of trees to a peatland will result in higher T rates relative to E as trees have higher LAI, access to deeper water tables and greater turbulent interactions (Admiral and Lafleur, 2007; Kettridge et al., 2013). However, Strilesky and Humphreys (2012) showed that overall ET rates were lower in a black spruce portion of a peatland compared to an open portion as a result of the decreased stomatal conductance of the black spruce compared to mosses, which lack stomatal controls, and as a result have been shown to significantly influence the ET budget within peatlands (Lafleur and Schreader, 1994; Kim and Verma, 1996; Heijmans et al., 2004). However, this study was performed in a

continental climate (Sonnentag et al., 2007) rather than the subhumid climate of the BP, which may result in greater E from both the open and treed portions as the atmospheric demand is higher (Devito et al., 2005).

Within the sheltered region, lower wind speeds and high temperatures suggest that ET will be driven by higher atmospheric demand due to the increased moisture holding capacity of the air as a result of increased temperatures (Figure 2-8B) (McNaughton, 1988; Cleugh, 1998). However, due to the high latitude and patchiness of the landscape, radiative shading can be significant control on evaporative dynamics within the sheltered region of BP peatlands, as shading potentially offset the increase in temperatures, and reduce available energy and photosynthetically active radiation (Cleugh, 1998; Kettridge et al., 2013). Diurnal variability throughout the day will increase air temperature and humidity as solar radiation and ET constantly act within the peatland (Caborn, 1957; McNaughton, 1988; Cleugh, 1998). This will create a dynamic relationship between air temperature and humidity, where increasing temperatures will increase the VPD, resulting in increased ET rates until the moisture demand of the air is met, which lowers the VPD (Runkle et al., 2014). However, more research is required to understand the diurnal variability of the interactions mentioned above.

Within the reattachment zone, higher turbulence suggests that wind stresses will control ET rates; however, this will strongly be influenced by the moisture conditions of the air entering the peatland (McNaughton, 1988; Petrone et al., 2007). When dry air is advected into the reattachment zone, high wind speeds and turbulence will increase evaporative rates. However, if moist air advection occurs, it will reduce evaporative demand compared to the dry air scenario as the air has little capacity to receive additional water vapor (Chapin et al., 2002). This suggests that

upwind topography and roughness should be taken into consideration when gauging the evaporative demand of the reattachment zone (Petrone et al., 2007).

2.4.3 Implications for land management strategies

Perched and isolated peatlands are prominent features of the BP (Metcalfe and Buttle, 1999; Riddell, 2008), and are important sources of water and carbon storage within the region (Kuhry et al., 1993; Timoney, 2003; Ferone and Devito, 2004). It is expected that the ubiquity of these peatlands throughout the BP landscape, despite the sub-humid climate (Devito et al., 2005), is a result of the sheltering of the surrounding forested landscape (Petrone et al., 2007). However, widespread landscape scale anthropogenic disturbances (in excess of 800 km^2; Government of Alberta, 2015) threaten such natural characteristics of the BP (Government of Alberta, 2015) by disrupting the fine balance between atmospheric fluxes of P and ET (Thompson et al., 2015; Riddell, 2008) within a region that is hydrologically driven by persistent water deficit conditions (Marshall et al., 1999; Devito et al., 2005). Thus, such industries should consider how landscape disturbance may be impacting the suppression of evaporative fluxes from these systems. For example, forestry clearcutting in the BP follow unclear criteria with regards to buffer designs around peatlands where buffer widths depend on features such riparian zone slope and the biotic habitat function with distances ranging from $x/h \geq 2$ (Murray and Buttle, 2002). However, van der Kindere and Ganapathisubramani (2018) observed that BFS transition characteristics were significantly dependant on the distance between the BFS and the FFS where short distances ($x/h \leq 4$) experienced less impacts of the sheltered region with turbulent intensities propagating further downwind compared to the longer distances of ($x/h \geq 4$). Furthermore, Wang and Tackle (1995) observed that shelterbelt porosity significantly influence streamwise wind velocities and characteristics of the BFS transition, where lower porosities result in lower wind speeds with less

"bleed flow" in the sheltered area and a more defined flow separation region. Therefore, forestry practices that have the potential to change approach flow turbulent properties, could significantly modify the BFS flow dynamics discussed in this study. If unaccounted for in forestry buffer designs, this could result in negative, unforeseen impacts on water and carbon fluxes within peatlands (Petrone et al., 2007; Plach et al., 2016). This warrant's further investigation in order to quantify the sensitivity of adjacent peatlands to turbulence associated with variable buffer lengths.

Oil sands development within the BP, also represents a major landscape disturbance impact (Daly et al., 2012; Rooney et al., 2012; Government of Alberta, 2015). Associated with this development, large-scale reclamation projects within the AOSR are required for mine closure plans as the lands have to be reclaimed back to an ecosystem with pre-disturbance functionality (i.e. a mosaic of uplands, wetlands and carbon accumulating peatlands) (Daly et al., 2012). However, the long maturation times for upland forests means that other methods such as steep slopes and rough terrain could be implemented in order to provide adequate regional roughness lengths to provide turbulent sheltering within the peatlands. Loureiro et al. (2009) investigated flow separation around a hill and found reattachment lengths between x/h = 2.5 - 5.8 for varying Reynolds numbers. However, the slope of the hill must be considered as the reattachment distance was measured from the point of separation and not the point where the slope meets the flat surface (Loureiro et al., 2009). If heterogeneous landscapes are implemented in reclamations strategies, evidence from this study suggests that surface roughness lengths should be considered when designing such landscapes as it can alter the evaporative demand expected affecting their sustainability under future climatic conditions. That is, increased surface roughness lengths within the peatland could decrease the spatial variability of aerodynamic drivers of ET within these peatlands compared to a smooth surface that could produce higher overall resistances to turbulent

transfer but would spatially be more variable. However, it is important to note that a combination of rough and smooth surfaces likely exists that would be the optimal design for such a peatland system, but this warrants further investigation.

2.5.0 Conclusion

Reduced streamwise velocities and higher vapor concentrations and temperatures in the sheltered region are followed by a sharp transition to increased streamwise velocities, turbulence and decreased vapor concentrations and temperatures in the reattachment zone. These microclimates produced by the BFS transitions result in a range of conditions that influence the atmospheric demand and stomatal characteristics of the vegetation, which in turn affects evaporative rates across the system. Furthermore, our results show that increasing the surface roughness leeward of a BFS decreases the size of the reattachment zone and the variability of aerodynamic resistances across the peatland surface. However, increased surface roughness did decrease the overall aerodynamic resistance of the surface. The consequences of the above findings on peatland evaporative demand is that the higher turbulence in the reattachment region will increase ET rates relative to the sheltered region. Moreover, increasing the surface roughness of the peatland results in greater overall evaporative demand from the surface, but decreases the spatial variability between the sheltered and the reattachment zones. The implications of this study to reclamation strategies is that microclimates are produced leeward of the BFS transitions, which result in spatially varying evaporative rates that could influence the success of these young reclaimed peatlands. However, our results show that by increasing the surface roughness leeward of the transition, the differences between these microclimatic zones can lessen and thereby decreasing the spatial variability of evaporation across the peatland surface thereby making the fluxes more predictable.

3.0 Microclimatic Effects of a Perched Peatland Gap

3.1.0 Introduction

The Boreal Plains region (BP) of the Western Boreal Forest (WBF) is composed of a heterogeneous mosaic of wetlands and upland forests, where wetlands account for approximately 50% of the natural landscape, of which approximately 90% are peatlands (Vitt et al., 1996). The sub-humid climate of the BP is characterized frequent water deficit conditions where potential evapotranspiration (PET) is greater than precipitation (P) on an annual basis, with wetlands being sustained by infrequent wet years on a 10 – 15 year cycle (Marshall et al., 1999; Devito et al., 2005). Perched peatlands are a common feature across the BP (Devito et al., 2012) and are hydrologically isolated from surface waters and the underlying water table. Perched peatlands are commonly observed above the regional water table (James, 2017; Riddell, 2008) and separated by an unsaturated layer, which acts to hydrologically isolate the peatland (Devito et al., 2012). As such, small perched peatlands have been shown to be controlled by climactic fluxes (P and ET) as opposed to ground water fluxes, making them more susceptible to climate variability and the delicate balance between P and PET within the BP region (Thompson et al., 2015; Riddell, 2008). Previous research on the hydrologic and microclimatic functioning of perched peatlands has shown that these systems in the BP have negative autogenic feedbacks that include turbulent sheltering, radiative sheltering and vegetative controls (James, 2017; Waddington et al., 2015). These feedbacks may serve to increase the resiliency of perched peatlands to evaporative losses (Petrone et al., 2007; Waddington et al., 2015; Hokanson et al., 2016; James, 2017; Chapter 2) by changing the ratio of AET to PET within these peatlands.

Examination of flow over a roughness transition can be conceptualized by combining and modifying the frameworks developed by Judd et al. (1998), Cleugh (1998) and Belcher et al.

(2003) as shown in Figure 3-1. Flow is divided into several distinct regions as it passes through a BFS – Gap – FFS sequence.

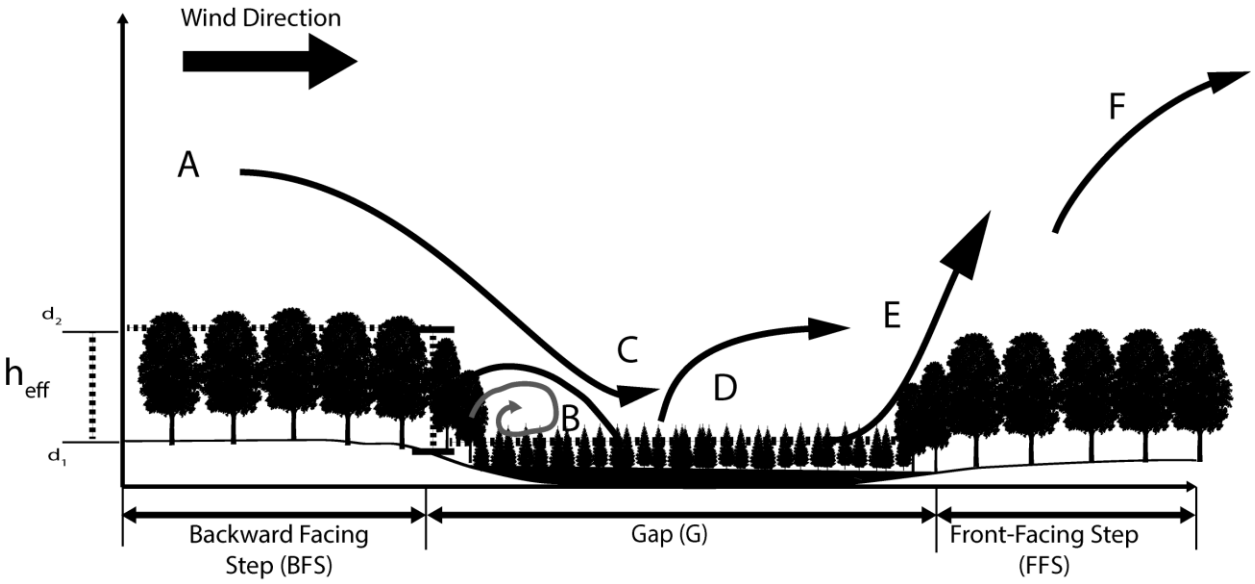

Figure 3-1: Schematic showing the unique zones created by flow adjusting over a backward facing step (BFS) transition, identifying the successive regions in the flow path: (A) approach flow; (B) sheltered region; (C) reattachment zone; (D) recovery region, (E) uplift region; (F) roughness change region (IBL).

Turbulent stresses vary across the gap surface as a result of the flow regimes produced by the roughness transitions (Figure 3-1). The turbulent state of the *approach flow* (A in Figure 3-1) has been shown to influence the lengths and characteristics of the *sheltered region* (B in Figure 3-1) and *reattachment zone* (C in Figure 3-1) (Simpson, 1989; Markfort et al., 2014; Chatziefstratiou et al. 2014; Kindere and Ganapathisubramani, 2018). The sudden change in the displacement height results in a decoupling of the flow profile from the surface, thereby increasing flow velocities and wind shear as it adjusts to the new surface element. The decoupling of the flow profile produces a region of reduced flow that is separated from the adjusting layer above (B in Figure 3-1), which results in a *sheltered region* that has reduced turbulent transport and increased scalar concentrations (Mcnaughton, 1988; Chapter 2). When mean *flow reattaches* with the new surface layer (C in Figure 3-1), it is characterized as having high flow velocities and turbulent

stresses producing an adverse pressure gradient resulting in flow reversals within the sheltered region. Development of the mean flow profile occurs after the reattachment zone, as the *flow recovers* (D in Figure 3-1) and surface turbulence equilibrates to the new surface layer and its roughness elements. The *uplift region* (E in Figure 3-1) that is characterised by high vertical wind speeds that lifts flow above and out of the step transitions, has been shown to effectively eject particles and scalars from the surface and into the atmosphere (Bergen, 1975; Goodrick et al., 2013; Belcher et al., 2008; Pruegor et al., 2008). The *roughness change region* (F in Figure 3-1) is where the flow adjusts to the roughness of the new surface with the development of an internal boundary layer (IBL). Height of the BFS influences reattachment distance, therefore the distance leeward of the BFS is scaled by using the effective canopy height (h_{eff}), where $h_{eff} = d_2 - d_1$, and d is the zero-plane displacement of the down-step (indicated with $_1$, and in our study, peatland) and the up-step ($_2$, forest) surfaces. Due to the complexites of BFS transitions, single point eddy-covariance (EC) measurements conducted within the flow transition are difficult to interpret and neglect the theoretical assumptions of a homgenous surface layer, zero mean vertial flow, and no vertical divergence of fluxes (Yang et al., 2006a; Lee, 2000; Paw et al., 2000). Therefore, 3-D computational fluid dynamic models that can resolve turbulence at a forest-to-peatland transition can be used to improve the understanding of flow dynamics within such environments (Bohrer et al., 2009).

Landscape heterogeneity, composed of a mosaic of largely peatlands and upland forests throughout the BP results in sharp transitions in displacement height that produce complex transitional flows and turbulent processes (Bou-Zeid et al. 2004; Markfort et al., 2010). Studies investigating flow separation over heterogeneous surfaces (e.g. Patton et al. 1998; Belcher et al. 2003; Yang et al. 2006b; Cassiani et al. 2008; Dupont and Brunet, 2008a; Fontan et al. 2013;

Chatziefstratiou et al., 2014) have identified transition structures by using the "step analogy" where there is either a forward-facing (FFS) or a backward-facing (BFS) depending step on the wind direction, with discussions being primarily focused on either the approaching or exiting flow (Detto et al. 2008; Panferov and Sogachev 2008; Chatziefstratiou et al., 2014). In complex terrain, such surface simplifications can be combined with a sequence of transitions such as BFS – Gap – FFS (e.g. a peatland surrounded by a forest) (Figure 3-1). As a result, land surface heterogeneity has the potential to act as a positive or negative autogenic feedback to atmosphere exchanges of momentum, heat and mass (Cleugh, 1996; Markfort et al., 2014; Plach et al., 2016, James, 2017; Chapter 1). For example, a negative autogenic feedback could be an uninterrupted transition (BFS - Gap), where reduced wind speeds in the *sheltered region* (B in Figure 3-1) could result in less movement of scalars away from the surface resulting in less evapotranspiration (Chapter 2; Cleugh, 1996). Conversely, if *flow reattachment* occurs (C in Figure 3-1), higher turbulent interactions with the surface could increase evaporative demand resulting in a positive autogenic feedback (James, 2017). Furthermore, due to the fragmented mosaic of the BP, there is the potential for a large portion of the landscape to be influenced by such variable feedbacks, making for spatially unpredictable fluxes from within these regions. Additionally, the small or short fetched nature of these peatlands means that transition regions can impact a large portion of them. Which increases the persistence of these hydrologically isolated perched peatlands across the landscape due to the moderated fluxes and decreased the ratio of AET:P; thereby increasing the resilient of the peatlands to the regional atmospheric demand of moisture.

Reduced computational time and costs have seen the emergence of Large Eddy Simulations (LES) as a practical research tool. However, many models use simplified structures such as transitions from blocks to flat surfaces or simplified canopy structures that assert drag on the mean

flow. Currently, semi-porous forest canopies are being modelled with the aid of computationally competent platforms and the ability to integrate vegetation profiles into LES has become available in models such as Regional Atmospheric Forest Large Eddy Simulation (RAFLES) (Bohrer et al., 2009) via the Virtual Canopy Generator (V-CaGe) (Bohrer et al., 2007). Allowing canopy integration into LES provides us with the ability to accurately model flow transitions as it has been observed that canopy influences on flow such as drag and through canopy flow, have a significant influence on the turbulent dynamics of transition flow (Markfort et al., 2014; Chatziefstratiou et al. 2014).

Increased natural resource activities, such as oil and gas extraction and oil sands development in the WBF has resulted in the disruption of landscape on a scale ranging from individual ecosystems to the scale of entire landscapes (Alberta Environmental Protection, 1998; Johnson and Miyanishi, 2008; Government of Alberta, 2015). Large-scale land reclamation projects such as mine closure plans in the Athabasca Oil Sands Region (AOSR) require the land to be returned to an equivalent land class i.e. the mosaic of wetlands and forests) (Daly et al., 2012). Therefore, it is critical to understand atmospheric transport processes and boundary layer interactions within complex terrain so that the autogenic feedbacks can be applied and considered in large-scale land reclamation designs where the success of the projects is crucial due to the high costs and to achieve land closer certification.

The persistence of small perched peatlands within the BP suggest that a combination of negative autogenic feedbacks exist that reduce the evaporative demand thereby increasing the sustainability of these systems across the BP (James, 2007). One such autogenic feedback is the fetch length of the peatland gap, as it has the potential to moderate turbulence and microclimate distribution across the entire peatland surface (Markfort et al., 2010). It is hypothesized that the

length of the gap has the potential to control flow reattachment dynamics where peatlands with gaps shorter than the reattachment zone would result in the entire peatland surface being detached from the mean flow profile (Troendle and Leaf, 1980; Golding and Swanson, 1978). This detachment could change the ratio of P to PET (Golding and Swanson, 1978; James, 2007). Furthermore, due to the stagnation point of FFS flows, the impacts of a BFS transition could be extended to peatlands with gap lengths slightly larger than the reattachment zone distance, where the combination of BFS sheltering and FFS stagnation point effectively increase the sheltered area of a peatland. Furthermore, it is unknown how FFS flow dynamics will respond to approaching flow that does not have the characteristics of a developed flow profile. Therefore, the objectives of this study are to: 1) examine the impact that fetch length has on turbulent processes and microclimates within a sheltered peatland; 2) Determine the impact that fetch length has on FFS dynamics and its impact to regional flow dynamics.

3.2.0 Materials and Methods

3.2.1 Site Description

This modeling study utilized synthetic simulation domains based on observed vegetation and meteorological parameters from an upland forest and peatland in the Utikuma Regional Study Area (URSA) of the BP in north-central Alberta. Meteorological data used to set up the site parameters that were prescribed for the upland-forest land classification components of the simulations (table 3-1) were obtained from the Pond 40 EC flux tower (56° 4'21.90" N, 115°28'33.30" W) in the Utikuma Region Study Area (URSA) near Utikuma Lake, northern Alberta. This site is dominated by dense, mature aspen (*Populus balsumifera* and *Populus tremuloides*), with mean canopy height of 25m and summertime mean LAI of 2.83 m^2/m^2. LAI measurements were collected using LP-80 LAI probe (Decagon Devices, Pullman, Washington, USA) during peak growing season at points

along a transect which captured site scale variability. The EC tower is located on gently sloped hills adjacent to low lying wetlands. The mean growing season temperature at this site is 13.4 ^{o}C; it is a dry site with ET:PET (EC method : Priestly-Taylor) ratio of 0.67. The EC system used to parameterize the upland was installed on a tower at a height of 23.5 m above the forest canopy, to produce a large enough footprint area to encompass landscape-scale variability (Brown et al. 2010, 2013; Devito et al., 2005; Petrone et al., 2015; Sutherland et al., 2017).

The peatland land classification used in this study was prescribed based on observations from an undisturbed moderate-to-rich peatland site, Super 8 (56° 4'48.80" N, 115°31'57.06" W), located in the Utikuma Region Study Area (URSA) near Utikuma Lake, northern Alberta. Super 8 is dominated by sparse *Picea glauca* along the north side and *Betula papyrifer* along the south end of the fen, underlain by Sphagnum mosses. For this study, the *Picea glauca* was used as the vegetation analog for the roughness parameterization with a mean vegetation height of 3.56 m and a mean summertime LAI of 1.75 m^2/m^2. LAI measurements in the peatland were collected using an LAI-2200C plant canopy analyzer (LI-COR: Lincoln, Nebraska, USA) during peak growing season with observation points following a transect throughout the site to capture site variability. The mean growing season temperature at this site is 12.6 ^{o}C, it is a relatively dry peatland compared to the other peatlands within the region with an ET: PET (EC method : Priestly-Taylor) ratio of 0.75 observed from an EC system measuring at a height of 6.5 m. The peatland is surrounded by a ~25 m sloping forest canopy dominated by (*Populus balsumifera* and *Populus tremuloides*) that exhibit a sharp transition from peatland to upland (Table 3-1).

Metoerological forcings used to prescribe V-CaGe were observed from eddy covariance systems where the upland measurments were collected using a LI-7500 (LI-COR: Lincoln, Nebraska, USA) open path IRGA paired with a CSAT3 3D sonic anemometer (Campbell

Scientific: Logan, Utah, USA) at a height of 23.5m scanning at 20 Hz during the growing season of 2008. While, EC measurements within the peatland were collected using an LI-7200 (LI-COR: Lincoln, Nebraska, USA) closed path IRGA and Windmaster Pro sonic anemometer (Gill Instruments: Lymington, Hampshire, UK) at a height of 6m, scanning at 10 Hz during the growing season of 2015. All flux data were processed into 30-minute average fluxes using, and filtered for periods of low atmospheric turbulence (u_*), corrected for density and sensor separation (Webb et al., 1980; Leuning and Judd, 1996; Petrone et al., 2015) and flux foot printing (Kljun et al., 2004). Final corrections and gap-filling followed the methods outlined in Petrone et al. (2001), Wilson et al. (2002) and Brown et al. (2010). Other meterological characteristics used force RAFLES were net radiation which was measured within the upland using an NR-Lite (Kipp Zonen; Delft, Netherlands) and in the peatland using a CNR4 (Kipp Zonen; Delft, Netherlands), both at the same height of the EC measurements. Albedo values were measured within the peatland and were supplemented with data from the literature for the upland (Table 1). Ground heat flux was calculated using ground heat flux probes (HFT3; Campbell Scientific: Logan, Utah, USA) for the upland while in the peatland ground heat flux was calculated with ground temperature profiles using the calorimetric method (Halliwell and Rouse, 1987; Petrone et al., 2000; Petrone et al., 2006).

Stand density, canopy height, and trunk taper functions were determined by averaging three random 10 m × 10 m sampling plots (Table 3-1). To remove smaller understory vegetation that was negligible for the simulation, trees with a breast height circumference less than 5 cm were ignored. Following Naidu et al. (1998), taper functions were calculated by producing a logarithmic regression between diameter at breast height and the height of the vegetation. Leaf area density (LAD) profiles were created by falling 2 - 3 trees per land class and measuring the height, trunk

diameter and crown diameter at 1 m vertical intervals. To obtain a crown volume, I assumed a uniform circular diameter of the canopy at 1 m interval, with all leaves being stripped and sorted based on the corresponding interval. For the peatland vegetation, every other 1 m section was used and interpolated between the heights due to the difficulty with transportation and needle removal. All vegetation was dried to standardize weight, from which a 10 g subsample was selected and measured using LI-3100C (LI-COR: Lincoln, Nebraska, USA) leaf area meter using a resolution of 0.1 mm^2. The area of the 10 g subsection was then used to scale-up the remainder of the sample and applied to the volume of the crown. To account for variability in tree heights and shape, vegetation samples from each land class were standardized into n = 100 point profiles to allow for averaging within tree types and for scaling purposes within V-CaGe.

3.2.2 Simulation setup

RAFLES was used to resolve flow inside and above heterogeneous three-dimensional (3-D) forest canopies by solving the 3-D Navier-Stokes equations on a rectangular, vertically stretched grid mesh. RAFLES incorporates a multi-layer, 3-D heterogeneous canopy, which allows modeling of drag, volume restriction, and energy fluxes to and from the vegetation canopy (Bohrer et al. 2009). Vegetation within RAFLES is parameterized using the shaved grid-cell method (Adcroft et al., 1997) in the V-CaGe sub-model to apply observed vegetation characteristics to the canopy domain (Chatziefstratiou et al. 2014).

The simulation domain used in this study was set to 1000 × 1000 × 1040 m^3 yielding 250 × 250 × 107 (x, y, z) cartesian grid points, with a horizontal grid resolution of 4 × 4 m^2, and vertical grid resolution of 2 m (to a height of 100 m). Above 100 m, a 10 % vertical stretching was applied for each consecutive vertical layer to a maximum vertical grid size of 25 m. Each simulation had a spin-up period lasting 2.5 hours with the observational period consisting of the last 30 minutes.

The model timestep is 0.05 seconds, with an averaged output every 2 seconds, for a total of 900 output files averaged into 30-minute flux periods used to calculate model parameters and align with EC measurements. Further details of RAFLES set-up and numerical schemes can be found in Bohrer et al. (2009).

3.2.3 Virtual canopy setup

The V-CaGe model was used to produce full, 3-D fields of numerical canopy elements and corresponding surface flux forcing for the peatland and forest land covers (Bohrer et al., 2007; Chatziefstratiou et al. 2014). The first RAFLES simulation used in this study is the long fetch scenario (Figure 3-2A), that consists of a rectangular forest block followed by rectangular peatland block (Chapter 2). The second RAFLES simulation used in this study consisted of two parallel peatlands referred to as the medium fetch (200 m fetch length) and short fetch (100 m fetch length) that were surrounded by a forest (Figure 3-2C, E). The medium and short fetch scenarios were combined and placed parallel to each other with respect to the streamwise velocities; this was done to reduce computation time and resources.

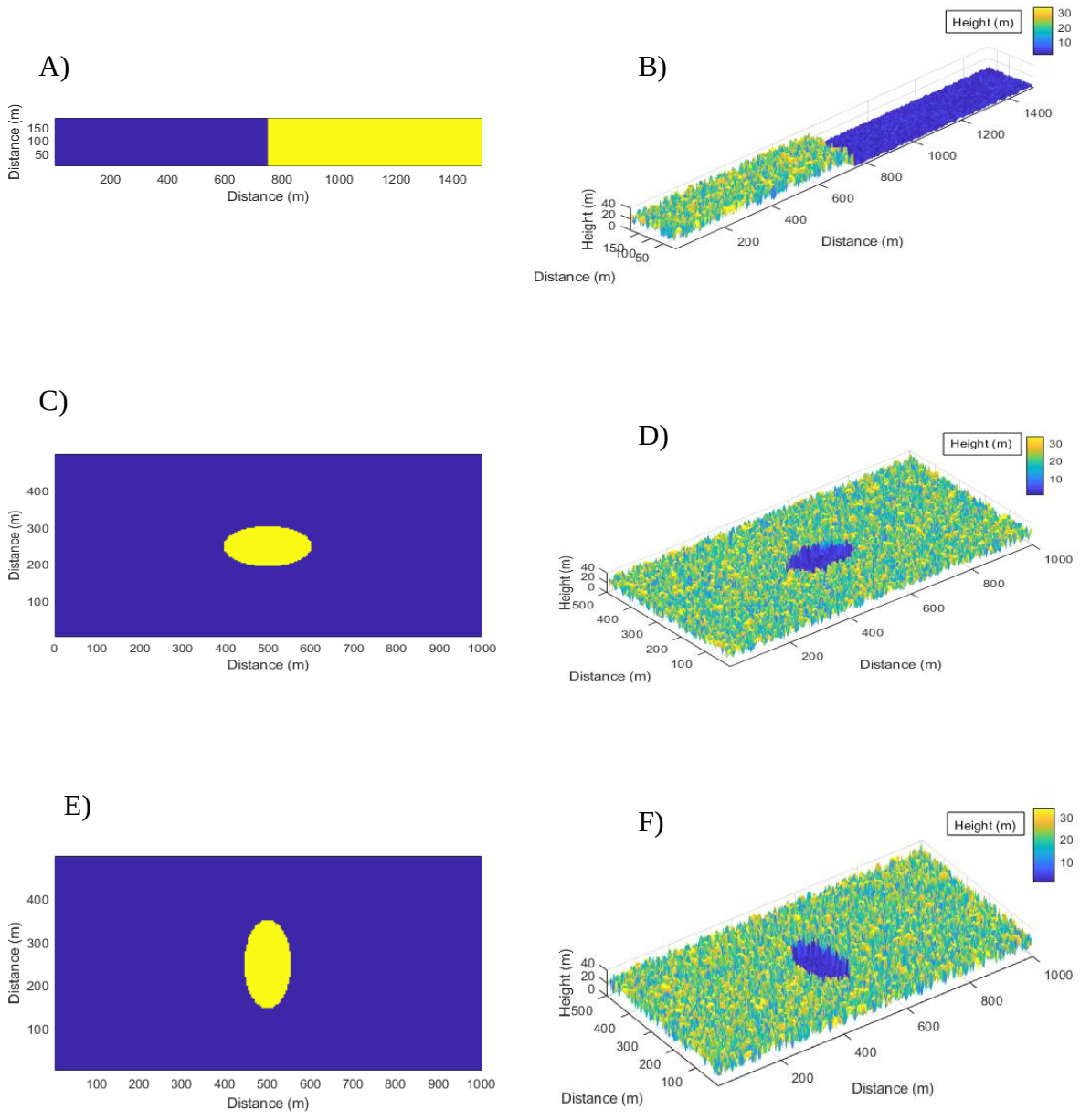

Figure 3-2: Model domains illustrating: A) the patch type of the long fetch simulation with purple representing the upland forest and yellow representing the peatland. Though the peatland gap occupies half of the downwind domain, the cyclic boundary conditions enforce an effective upland forest (in the upwind edge) at the downwind edge of the simulation domain; B) the canopy heights associated with patch types of Figure 2A; C) the patch type of the medium fetch simulation with purple representing the upland forest and yellow representing the peatland; D) the canopy heights associated with patch types of Figure 2C; E) the patch type of the short fetch simulation with purple representing the upland forest and yellow representing the peatland; and F) the canopy heights associated with the patch types of Figure 2E.

V-CaGe was used to prescribe the vegetation and meteorological parameters for each roughness case within RAFLES (Table 3-1). The Bowen ratio (H/LE) and the sum of turbulent fluxes ($H + LE$) were measured using an eddy covariance (EC) tower within each patch type at the sites described above during the summers of 2008 and 2015, where *H* and *LE* are the sensible and latent heat flux, respectively. To standardize the data between sites, the average of daytime (10:00-17:00) conditions during the growing season (Julian day 152-243) were used to parameterize the fluxes within each patch type.

Table 3-2: Values used for patch type parameterization in V-CaGe. [1]Values taken from Thompson et al. (2015).

Canopy parameter	Forest Upland	Peatland
Stand density (stems/ha)	2600	2700
Mean canopy height (m)	25	3.56
Std of canopy height	8.9	1.5
Mean LAI (m^2 /m^2)	2.83	1.75
Std of LAI	1.38	0.61
Mean Bowen ratio	1.1	0.81
Std of Bowen ratio	0.65	0.73
Mean canopy-top total flux forcing (W/m^2)	323.84	397.5
Std of canopy-top total flux	118.89	221.28
Mean Albedo	0.16 [1]	0.12
STD Albedo	0.01 [1]	0.3

3.2.4 Initial conditions and forcing

The RAFLES simulation was initialized using horizontally homogeneous wind, humidity, and temperature profiles. Due to the absence of high-resolution vertical wind profiles, wind profiles were prescribed using the Obukhov similarity theory as it describes mean flow and turbulent

properties within the atmospheric sublayer (Monin and Obukhov, 1954). A simplified equation for the surface stress (drag coefficient assumed constant, is removed from the equation) is:

$$u^* = \frac{\kappa \overline{u_z}}{ln\left(\frac{z-d}{z_0}\right) - \psi_m\left(\frac{z-d}{L}\right) + \psi_m\left(\frac{z_0}{L}\right)} \quad (1)$$

where u_* is the frictional velocity, κ is the von Kármán constant (0.41), $\overline{u_z}$ is the mean streamwise wind velocity at z height above the canopy, L is the Obukhov length, d is the displacement height estimated as $d=2/3h$, or calculated using (equation 9), z_o is the roughness length estimated as $z_o=0.1 \times h$ or calculated using (equation 10) where h is canopy height. Paulson (1970) described the atmospheric-stability correction function ($\psi_m(x)$) for unstable atmospheric conditions ($z/L < 0$) as:

$$\psi_m(x) = 2ln\left[\frac{1+(1-16x)^{\frac{1}{4}}}{2}\right] + ln\left[\frac{1+(1-16x)^{\frac{1}{2}}}{2}\right] - 2\,tan^{-1}\left[(1-16x)^{\frac{1}{4}}\right] + \frac{\pi}{2} \quad (2)$$

Where x is either $(z - d)/L$, or z_o/L.

I applied Equation 1 to observed conditions from the upland EC tower at a characteristic time when h = 25 m, u_* = 0.53 ms^{-1}, L = -124.11 m using the same data selection criteria that was used for the selection of V-CaGe surface fluxes. Vertical profiles of potential temperature and water vapor mixing ratio were prescribed using observed data from Fort Smith, Alberta (YSM) atmospheric sounding station (data obtained from the University of Wyoming database: http://weather.uwyo.edu/upperair/sounding.html) on August 31st, 2015 at 12:00 PM. All profiles were linearly interpolated at 25 m intervals to fit the vertical forcing prescription of RAFLES. Temperature, and humidity profiles, and turbulent wind fields were allowed to evolve during the spin up of the simulation. Following a spatial distribution described above, simulation forcing's included prescribed surface fluxes from each soil surface and vegetation-containing voxel, while

lateral wind nudging was used to maintain the prescribed mean vertical wind profile aloft (above a height of 4*h*). This is equivalent of prescribing a geostrophic wind gradient but does not require a-priori knowledge of the total surface drag force to balance the geostrophic wind.

3.2.5 Analysis of simulation results

Canopy aerodynamic resistance to moisture transfer was calculated through the moisture diffusion equation:

$$r_q = -Lv\rho\left(\frac{q_a - q_c}{LE}\right) \quad (3)$$

where r_q is the canopy aerodynamic resistance to moisture transfer, Lv is the latent heat of vaporization of water, ρ is air density, q_a is the water vapor mixing ratio at a height above the canopy, q_c is the canopy-air water vapor mixing ratio, and LE is the net surface + canopy latent heat flux.

3.3 Results

3.3.1 Flow Dynamics and Gap Length

BFS transitions produce high turbulence and flow acceleration that are directed into the peatland (Figure 3-3, 3-4). Similar flow acceleration rates are experienced entering each of the peatlands; however, greater turbulence is experienced in the medium fetch peatland compared to the short and long fetch peatlands (Figure 3-3). The reattachment zone distance is similar within each of the fetch lengths, where reattachment distances of between $x/h_{eff} \approx$ 3-8 are observed (Figure 3-3, 3-4, 3-7A). However, maximum downward velocities occur at a further distance leeward of the BFS in the medium fetch peatland compared to the short and long fetch peatlands (Figure 3-7B). Streamwise wind velocities at the surface of the peatland are suppressed within the short and medium fetch peatlands compared to the long fetch simulation, where at $x/h_{eff} = 8$, $\overline{U}_h/\overline{U}_0 \approx 0.35$, 0.41 and 0.55 for the short, medium and long fetch simulations, respectively (Figure 3-7A).

Streamwise surface velocities continue to accelerate within the long fetch simulation until $x/h_{eff} \approx$ 15, which exceeds the fetch length of the short simulation and is just under the fetch distance of the medium length simulation. Flow acceleration within the short and medium fetch peatlands continues until $x/h_{eff} \approx 6$ and $x/h_{eff} \approx 12$, at which point streamwise velocities equalize in the short fetch peatland and begin to decelerate in the medium fetch peatland. Surface turbulence $\sigma(w_h)$ is lower and does not reach an equilibrium in the short and medium fetch length peatlands compared to the long fetch peatland, which equilibrates at $x/h_{eff} \approx 15$ (Figure 3-7C). Although $\sigma(w_h)$ is reduced in the short and medium fetch simulations, similar trends across the reattachment surface are observed with peak $\sigma(w_h)$ occurring in the reattachment region within each peatland.

Surface vertical wind velocities of the peatland are similar between all fetch lengths (Figure 3-7B). Similar maximum uplift rates of $\bar{w}_h \approx 0.19$, 0.2 and 0.21 ms^{-1} are experienced in the sheltered region of the short, medium and long fetch peatlands, respectively. Furthermore, similar peak downward velocities occur in the reattachment zone of the peatlands with $\bar{w}_h \approx$ -0.19, -0.2, -0.25 ms^{-1} at $x/h_{eff} \approx 5$, 6, 4 for the short, medium and long fetch peatlands, respectively. Surface level vertical wind velocities fully recover and reach an equilibrium in the long fetch peatland, while no flow recovery is observed in the short and medium fetch peatlands (Figure 3-7B).

Within the long fetch simulation, the effect of the uplift region leading towards the FFS can be observed (Figure 3-7B) where vertical surface velocities begin to increase at from $\bar{w}_h \approx 0$ at $x/h_{eff} \approx 55$ and reach a maximum of $\bar{w}_h = 0.2$ ms^{-1} at $x/h_{eff} \approx 64$. Following this, there is a region of downward flow at the FFS that is observed within all fetch lengths scenarios. Furthermore, the magnitude of the uplift region in the medium and long fetch peatlands is greater than the short fetch peatland. Lateral flow convergence is observed towards the FFS throughout the medium and

in the corners of the short fetch peatlands, while no trends are observed in the long fetch scenario (Figure 3-5). Within all fetch lengths, flow penetrates $x/h_{eff} \approx 5$ into the FFS, where flow either

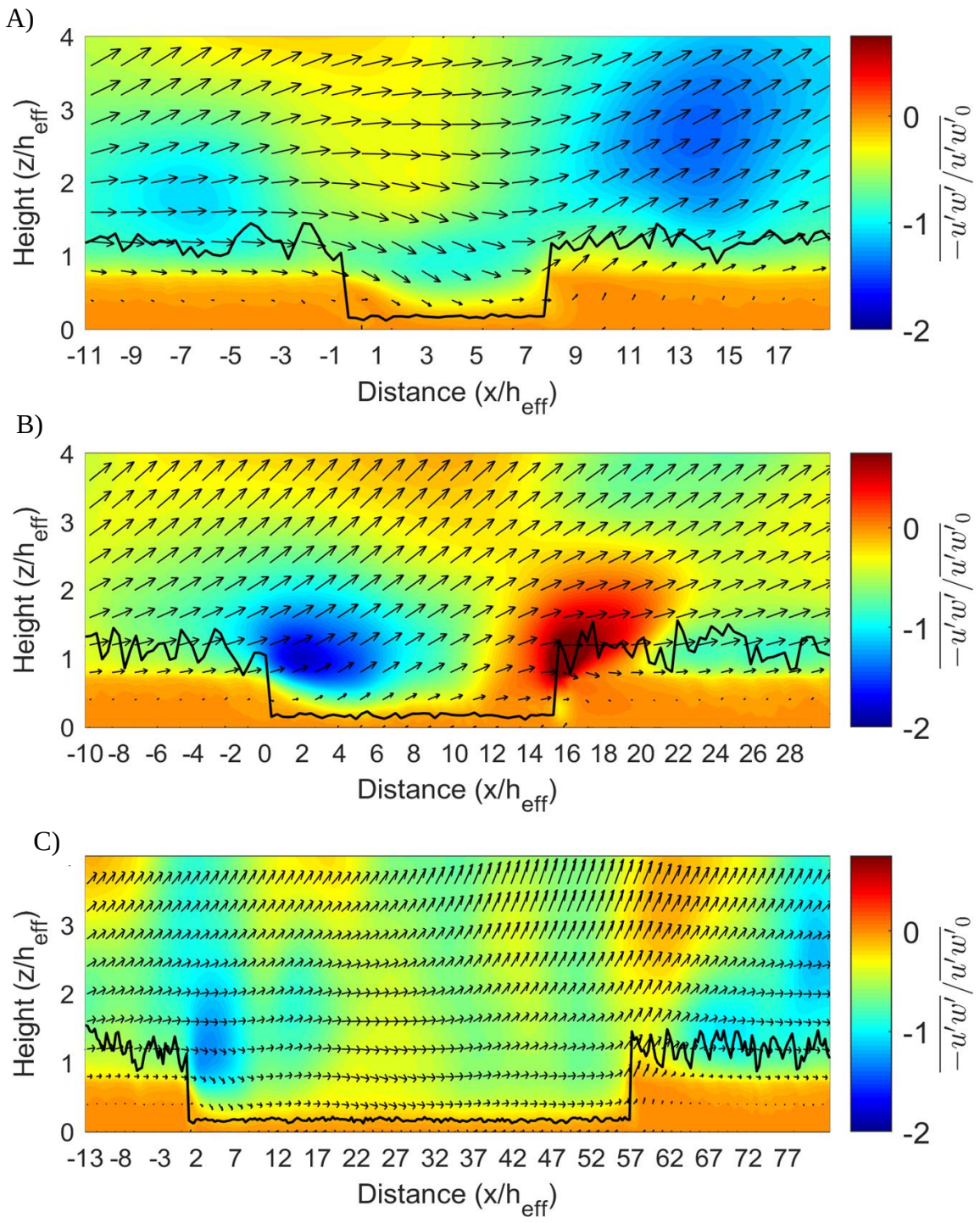

Figure 3-3: Cross section of Reynolds stress ($\overline{u'w'}$) normalized by the Reynolds stress at twice the upland canopy-top height (colormap), where arrows mark the wind velocity along the streamwise and vertical components. The x-axis marks the downwind horizontal distance from the BFS transition relative to the canopy height, h_{eff}. The z-axis marks the vertical elevation above ground relative to h_{eff}. Solid black line in each panel denotes the forest canopy top. (A) The short fetch length peatland, (B) The medium fetch length peatland. (C) The long fetch length peatland.

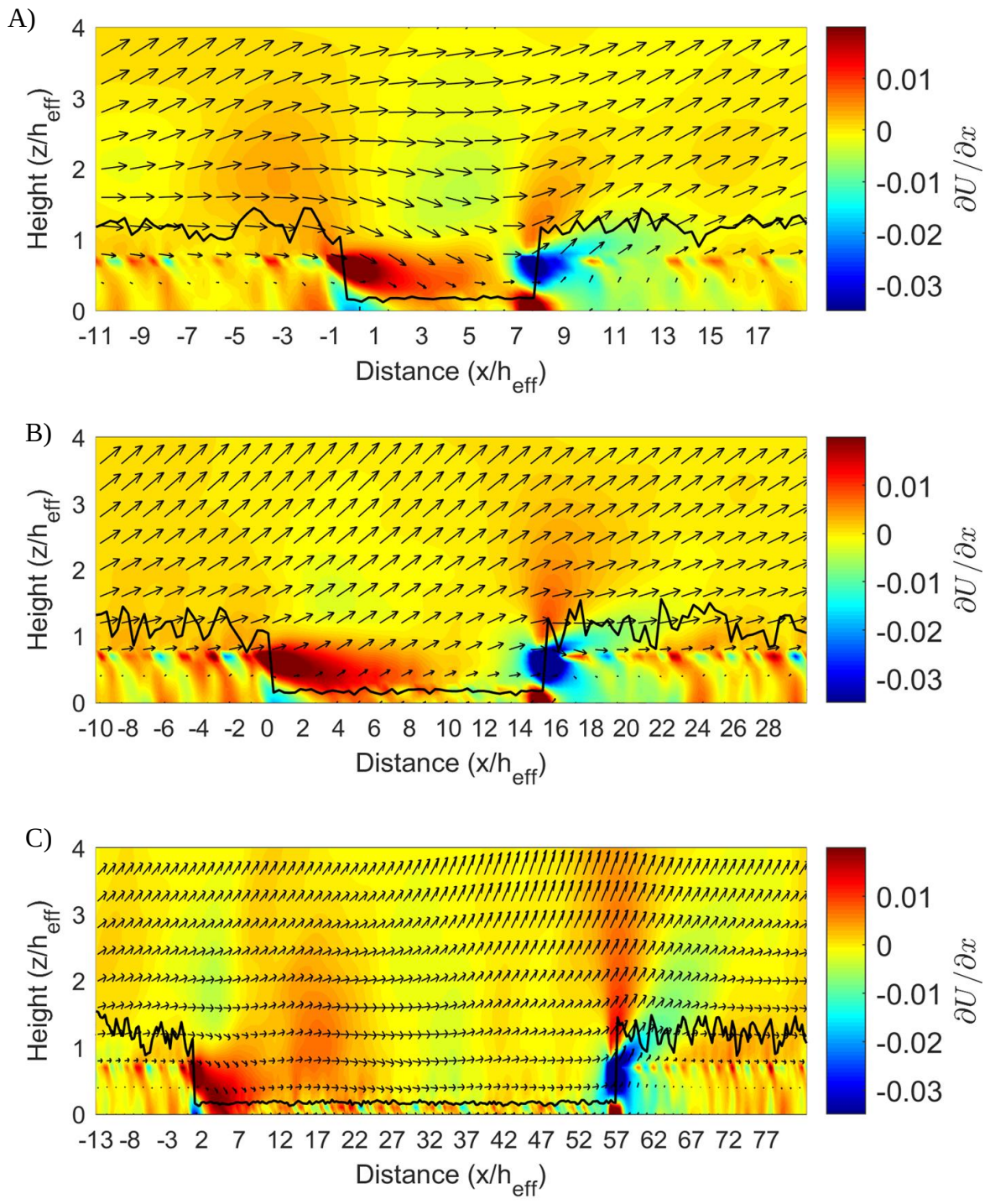

Figure 3-4: Cross section of the acceleration of wind in the streamwise direction $\left(\frac{\partial u}{\partial x}\right)$ *[ms*$^{-1}$*], where arrows mark the wind velocity along the streamwise and vertical components. The x-axis marks the downwind horizontal distance from the BFS transition relative to h. The z-axis marks the vertical elevation above ground relative to* h_{eff}*. Solid black line in each panel denotes the forest canopy top. Color map marks the acceleration of wind in the streamwise direction. (A) the short fetch length peatland, (B) the medium fetch length peatland and (C) the long fetch length peatland.*

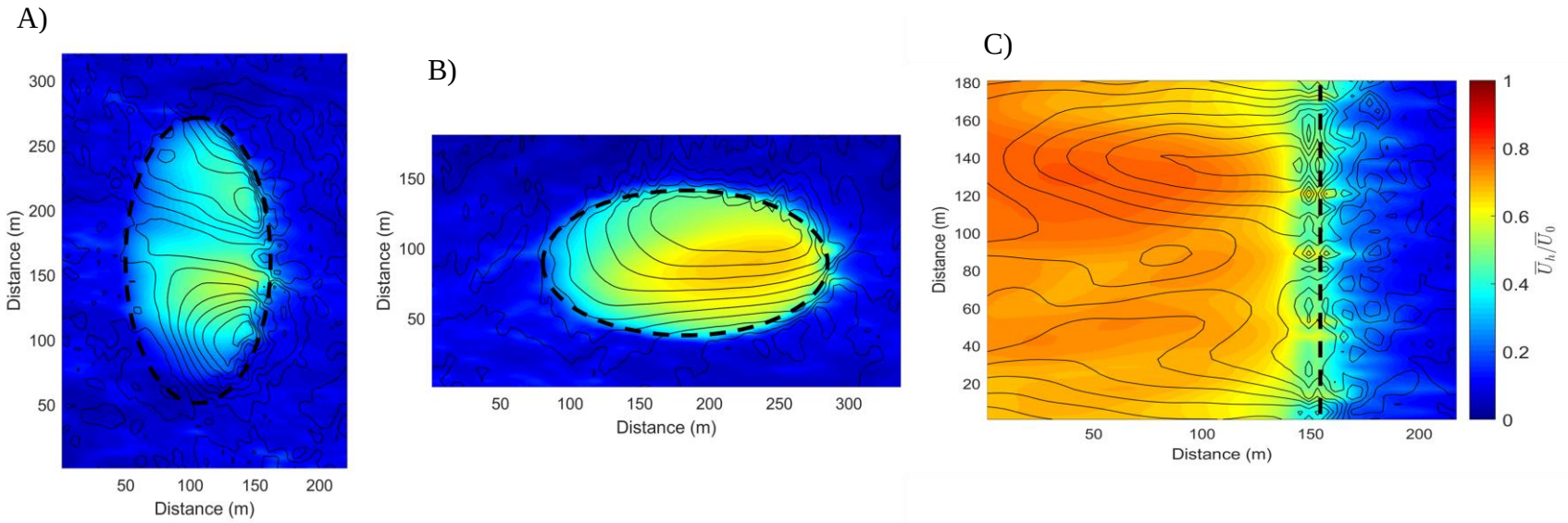

Figure 3-5: Top views of streamwise wind velocities measured at z/h_{eff} = 0.5 and normalized by mean streamwise velocities at a height of z/h=2 and the contours are of lateral flow velocities measured at z/h_{eff} = 0.5. The x-axis marks the distance in m. The y-axis marks the distance in m. Dashed black line in each panel denotes the boundary between the peatland and upland forest. Color map marks the of streamwise velocities measured at z/h_{eff} = 0.5 and normalized by mean streamwise velocities at a height of z/h=2. Contours mark lateral flow velocities measured at z/h_{eff} = 0.5. Panel (A) the short fetch length peatland, (B) the medium fetch length peatland and (C) the long fetch length peatland.

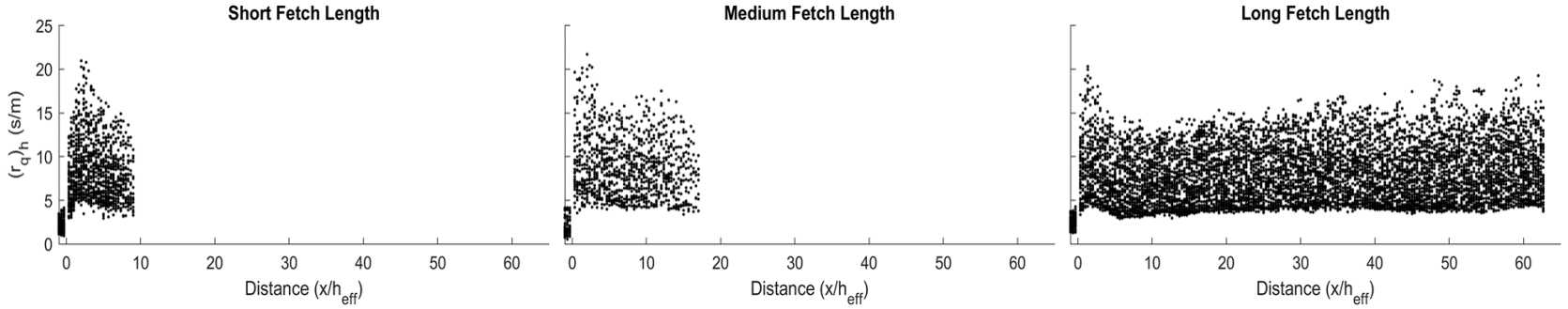

Figure 3-6: Canopy resistance to moisture transfer (sm^{-1}) measured at height h within the peatlands across short, medium and long fetch cases (left to right) with the x-axis being the distance from the BFS transition relative to the mean canopy height of the upland forest.

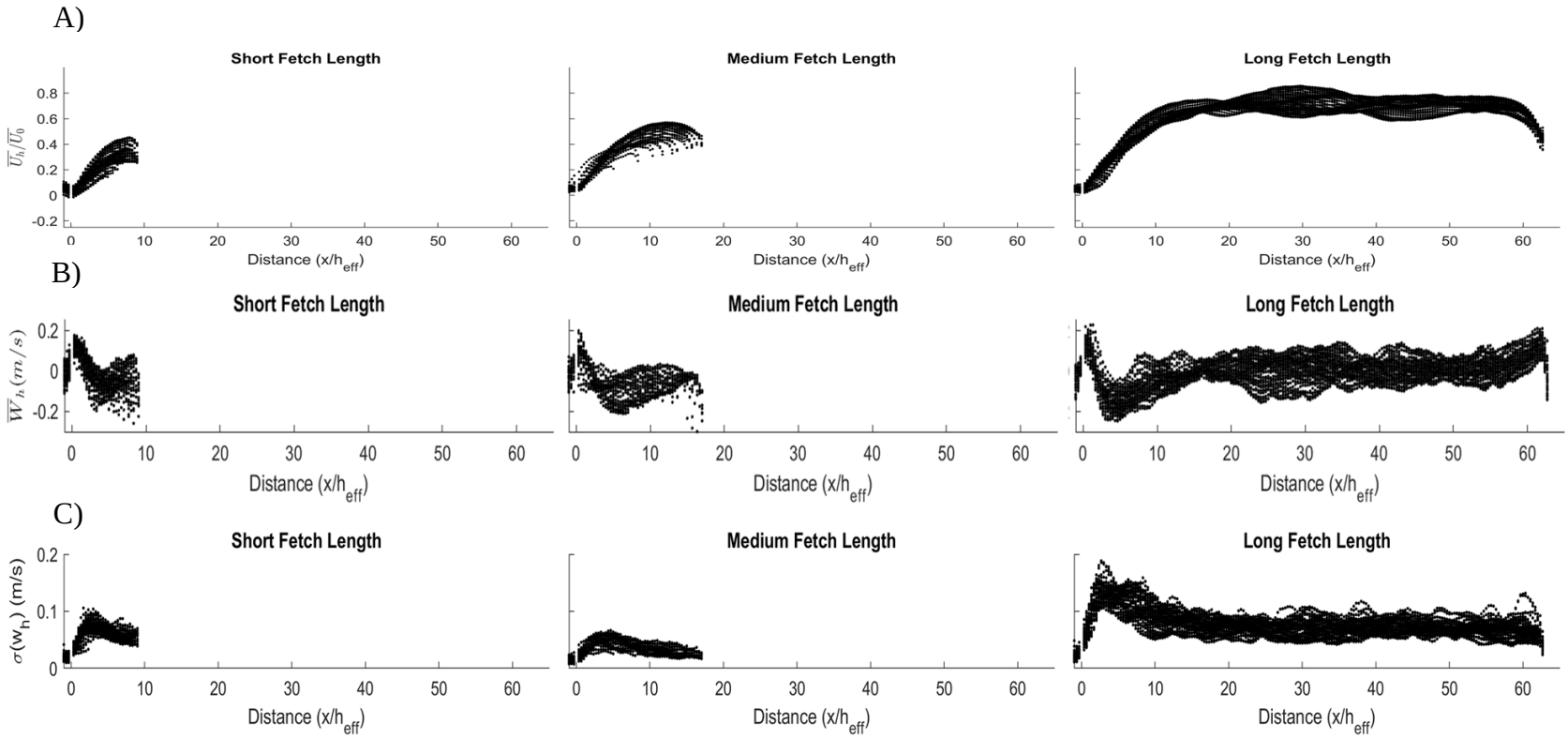

Figure 3-7: A) Is the mean streamwise velocities ($\overline{U}$) [ms^{-1}] measures at height h across short, medium and long fetch cases (left to right) with the x-axis being the distance from the BFS transition relative to the mean canopy height of the upland forest. B) Is the mean vertical windspeed ($\overline{w}$) [ms^{-1}] measured at height h across short, medium and long fetch cases (left to right) with the x-axis being the distance from the BFS transition relative to the mean canopy height of the upland forest. C) Is the standard deviation of vertical flow ($\sigma(w_h)$) [ms^{-1}] measured at height h across short, medium and long fetch cases (left to right) with the x-axis being the distance from the BFS transition relative to the mean canopy height of the upland forest.

accelerates above or decelerates below and into the forest the height of peak leaf area density (Figure 3-4). Mean streamwise wind velocities above the forest canopy measured at $z/h_{eff} = 2$, are $\bar{U}_h = 3.38, 3.89, 3.29\ ms^{-1}$ for the short, medium and long fetch scenarios, respectively. Stronger turbulence and flow acceleration suggest that the medium and long fetch simulations experience a stronger and more defined IBL development above the FFS (Figure 3-3, 3-4).

3.3.2 Fetch Length and Canopy Resistance to Moisture Transfer

Increased water vapor concentrations (Figure 3-8) and air temperatures (Figure 3-9) are observed in the sheltered region of each of the fetch length scenarios. Although surface water vapor concentrations and temperatures vary with distance from the BFS as reattachment dynamics control the scalar values, surface water vapor concentrations and temperatures are not modified by variable fetch length. Both water vapor concentrations and air temperatures are decreased in the forest until $x/h_{eff} \approx 5$ leeward of the FFS compared to the average values of the forest. Maximum surface r_q rates of r_q = 20.3, 21.7, 21.0 sm^{-1} are observed in the sheltered region for the short, medium and long fetch peatlands, respectively. Within each of the peatlands, r_q rates decrease in the reattachment region and then equalize in the recovery region (Figure 3-7). Differences between r_q rates are observed between flow regions (Chapter 2), while no differences are observed variations in fetch lengths.

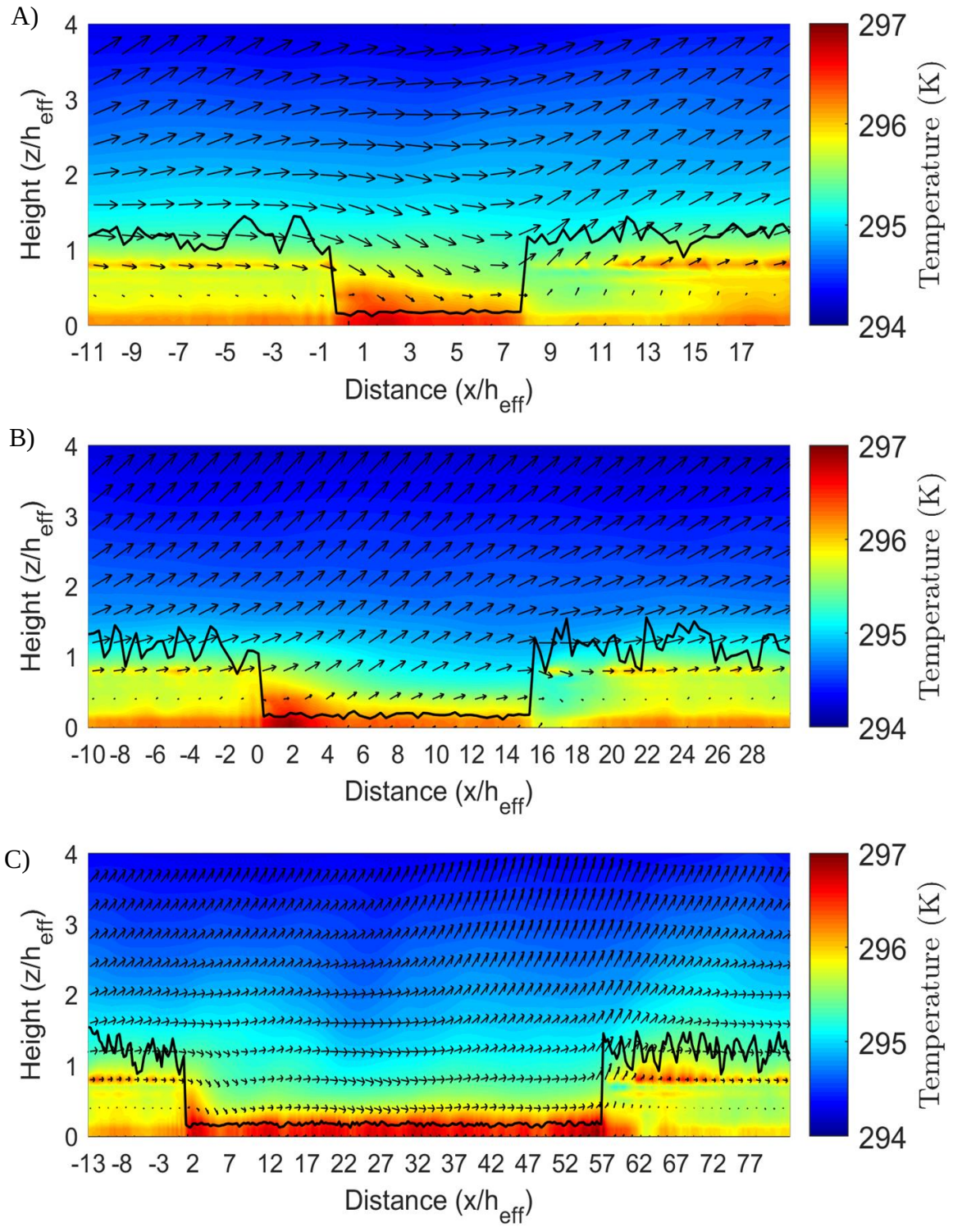

Figure 3-8: Cross section of air temperature [K], where arrows mark the wind velocity along the streamwise and vertical components. The x-axis marks the downwind horizontal distance from the BFS transition relative to h. The z-axis marks the vertical elevation above ground relative to h_{eff}. Solid black line in each panel denotes the forest canopy top. Color map marks the air temperature. (A) the short fetch length peatland, (B) the medium fetch length peatland and (C) the long fetch length peatland.

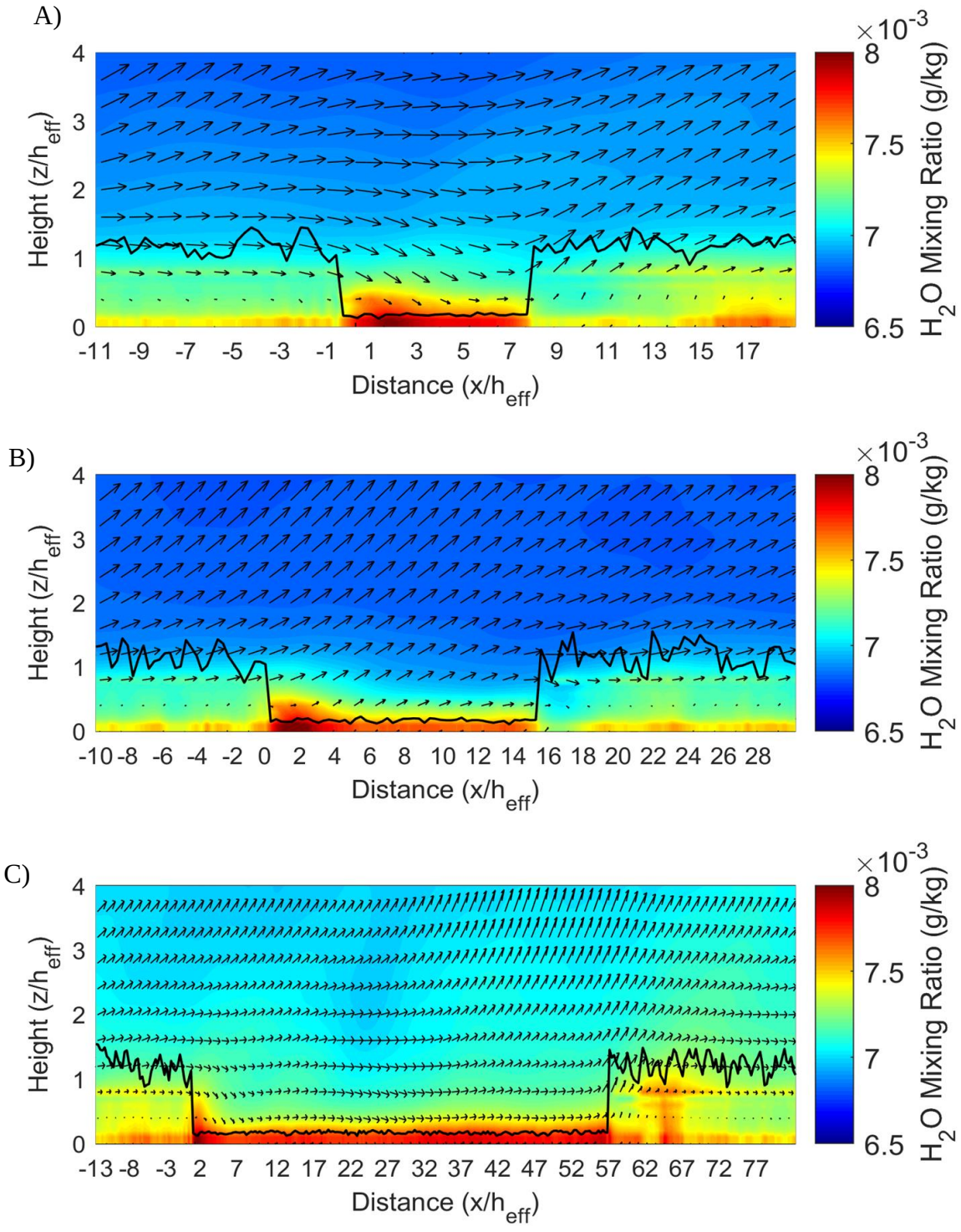

Figure 3-9: Cross section of the mixing ratio of water vapor [g/kg], where arrows mark the wind velocity along the streamwise and vertical components. The x-axis marks the downwind horizontal distance from the BFS transition relative to h. The z-axis marks the vertical elevation above ground relative to h_{eff}. Solid black line in each panel denotes the forest canopy top. Color map marks the water vapor mixing ratio. (A) the short fetch length peatland, (B) the medium fetch length peatland and (C) the long fetch length peatland.

3.4.0 Discussion

3.4.1 Effects of fetch length on micrometeorological interactions

It was found that the gap's fetch length had a strong impact on the vertical wind and turbulence over the gap. In the medium fetch scenario, faster streamwise wind velocities above the forest canopy are attributed to increased lateral flow convergence at the FFS (Murphy et al., 1983). The narrow shape of the medium fetch peatland increases the streamwise wind velocities by funneling the wind within the peatland towards and above the FFS (Jones et al., 2003; Damschen et al., 2014), which produces greater turbulence (Figure 3-3) between z/h_{eff} = 0.6-2 of the FFS. This results in less vertical uplift above the FFS compared to streamwise velocities when related to the short or long fetch scenarios (Figure 3-3). Therefore, the FFS shape has a greater influence on the regional streamwise velocities than the fetch length of the peatland. Furthermore, the short fetch scenario contains a larger ratio of the forest:peatland in the streamwise direction compared to the medium and long fetch scenarios which results in an aerodynamically rougher surface that results in slower above canopy wind speeds (Monin and Obukhov, 1954). This suggests that the internal shape of the peatland and FFS may play a large role in the dynamics of local wind velocities. Additional factors that characterize peatland FFS shapes and geometries and that I did not test in this experiment, such as the ratio between length and width of the peatland and the shape of the edges of the peatland such as square/flat or rounded corners, may further affect the results.

FFS properties have been heavily studied (c.f.. Cornelis and Gabriels, 2004; Belcher et al., 2008; Dupont and Brunet 2008a, b; Ruck et al., 2010; Belcher et al. 2012; Goodrick et al., 2013; Chatziefstratiou et al. 2014) and have determined that an increase in porosity of the FFS results in greater dissipation of flow through the FFS leading to a reduction in the size and strength of the recirculation region and the velocities of flow within the uplift region (Cornelis and Gabriels, 2004;

Ruck et al., 2010). Natural transitions from peatlands or other patchy landscapes to a forest may have a gradual transition where the transition vegetation acts to modify the porosity of FFS; thereby influencing the turbulent dynamics of the FFS (Ruck et al., 2010). However, for our simulations I chose the simple case of sharp transition where the peatland and forest are not separated by a transition vegetation region.

Flow reattachment leeward of the BFS is dependant upwind factors such as the geometry of the BFS, state of the boundary layer at the separation point, freestream turbulence, and upwind surface roughness (Markfort et al., 2014; Kindere and Ganapathisubramani, 2018). As such, the medium length peatland has a greater reattachment distance and higher turbulence compared to the short and long fetch simulations, which is consistent with previous studies as the medium fetch scenario had faster above canopy windspeeds (Simpson, 1989). Furthermore, this supports the notion that BFS flow separation is typically governed by upwind factors as it is not correlated to fetch length. However, our study shows that FFS shape can influence regional flow dynamics where a narrower FFS can promote faster flow out of the peatland. This has the potential to impact BFS transitions downwind by either decreasing or increasing the wind speeds and boundary layer heights, resulting in less predictable flow dynamics in downwind peatlands (Bou-Zeid et al., 2004; Kindere and Ganapathisubramani, 2018). Therefore, it is imperative to have a better understanding of how peatlands or other similar structures influence the dynamics of regional flow within the mixing layer.

3.4.2 Fetch length effects on evaporative demand

Surface resistance to moisture transfer does not vary with fetch length. As such, flow separation is the largest control on r_q across the peatland surface, where the sheltered region experiences the highest resistance rates compared to the reattachment and recovery regions (Chapter 2). Although

fetch length does not have an impact on the distribution of r_q rates leeward from the BFS, it may be advantageous to have the fetch of the peatland short enough that the sheltered region encompasses the entire peatland in order to minimize water loss. However, this may increase vapor concentrations and air temperatures (McNaughton, 1988; Cleugh, 1998) within the peatland that could produce unfavorable conditions that increase evaporative demand by altering the conditions that driving vegetation to atmospheric exchanges (Strilesky and Humphreys, 2012; Runkle et al., 2013).

Gap lengths between *5x/h* and *12x/h* have been shown to have other impacts on the landscape such as greater snow accumulation within the gap (Troendle and Leaf, 1981) and modifying the radiative budget (Cleugh, 1998; Kettridge et al., 2013). These can further affect the moisture availability at the peatland surface that can influence ET rates throughout the growing season. Troendle and Leaf (1981) observed that snow accumulation is higher in shorter fetch landscapes as the reduced turbulence and wind velocities reduce snow redistribution across the landscape, which effectively traps snow within the gap. Increased snow accumulation within the peatland would increase annual hydrologic input. This could shift the ratio of PET:P within the peatland, thereby increasing the resiliency of the peatland to the evaporative stresses of the sub-humid climate of the BP. Depending on the orientation of the peatland relative to the solar zenith angle, shorter fetch peatlands in the BP also have the potential to have a larger portion of their surface shaded from incoming radiation as the high latitude allows for greater BFS shading distances (Kettridge et al., 2013). The shorter the fetch length is with respect to this shading angle, the greater the portion of the peatland that would be shaded. Such radiative shading would decrease ET and surface heating by reducing available energy. However, interactions of radiative shading

with turbulent sheltering and its long-term effects on peatlands are unknown and warrants further investigation.

3.4.3 Implications of Fetch Limited Peatlands on Land Management Strategies

Perched peatlands are common features of the BP (Metcalfe and Buttle, 1999; Riddell, 2008) and are an important source of water and sink of carbon (Kuhry et al., 1993; Timoney, 2003; Ferone and Devito, 2004). Despite the sub-humid climate and persistent water deficit conditions (Marshall et al., 1999; Devito et al., 2005; Devito et al., 2015), peatlands are present throughout the BP landscape and their persistence is aided by turbulent sheltering from the surrounding forested landscape (Petrone et al., 2007). However, anthropogenic disturbances, covering more than 901 km^2 in Alberta alone (Canadian Oil and Natural Gas Producers, 2018) threaten the natural stability of the BP (Government of Alberta, 2015) by disrupting the delicate balance of P and ET (Thompson et al., 2015; Riddell, 2008). Therefore, industrial disturbances should consider how landscape alterations may impact the turbulent processes and consequently the change in evaporative demand in the surrounding landscape. For example, forestry practices in the BP often use the cutblock technique, which typically follow straight lines that cut square or rectangular features into the landscape. Our research suggests that a flat FFS would reduce above forest velocities compared to a peatland that experiences greater funneling of flow out of the peatland. However, disturbances of this nature should be investigated further as it is unknown if there is a relationship between the ratio of gap length and width and the influence of rounded corners. Furthermore, the downwind landscape should be considered when creating such a disturbance as disturbances upwind can change the turbulent processes of downwind ecosystems.

Oil extraction within the BP represents a significant landscape disturbance (Daly et al., 2012; Rooney et al., 2012; Government of Alberta, 2015). As a result of this development,

landscape-scale reclamation projects within the region are required to return the landscape back to an equivalent pre-disturbance functioning ecosystem (i.e., a mosaic of uplands, wetlands, and carbon accumulating peatlands) (Daly et al., 2012). Our research suggests that it is important to design the geometry of such systems with BFS and FFS flow dynamics in mind, as edge designs can influence flow dynamics at a regional scale. By not considering the turbulent impacts of peatland edge designs; faster windspeeds could result in higher vegetation stresses (Cleugh, 1998), snow redistribution (Troendle and Leaf, 1981), and excessive seed dispersion (Bohrer et al., 2008), which could influence the successional trajectory and success of large-scale integrated landscape reclamation projects. Furthermore, this research suggests that one regional roughness value may not be an adequate prescription to estimate regional wind velocities as peatlands with the same area and therefore regional roughness (Lettau (1969) and Kondo and Yamazawa (1986) methods), can produce different regional wind dynamics due to the orientation and geometry of their transition steps. The long maturation times of constructed upland forests means that peatland-upland edges could be defined by hillslopes or other constructed barriers, controlling evaporative demand in the peatland. Furthermore, the water demands of reclaimed peatlands expected to change as the development of the vegetation on the surrounding uplands will intercept more precipitation and use more ground water in order to meet the demands of the vegetation. Consequently, reducing the ground water inputs into these peatlands resulting in greater water stresses within the peatlands. Therefore, designing these peatlands with the understanding of the spatial distribution and drivers of evaporative stresses could ensure the long-term success and or explain the spatial evolution of vegetation within these peatlands.

3.5.0 Conclusions

Flow re-attachment dynamics are similar between peatlands with different fetch lengths as BFS flow dynamics are typically determined by upwind surface and flow characteristics. As a result, similar surface resistance rates to moisture transfer are observed between all fetch lengths. Our study also demonstrates that differences in above canopy wind speeds occurred when peatland geometry and FFS shape encouraged funneling of flow through the peatland, and above to the forest canopy. Such dynamics have the potential to influence the turbulent processes and evaporative stresses of downwind ecosystems. However, the sensitivity of the above canopy flow dynamics to changes in peatland geometry and FFS shape warrants further investigation as its direct investigation was out of the scope of this study. The findings of this study pose significant implications to land management and reclamation strategies in that although the fetch length of a peatland does not influence the flow recovery dynamics of a BFS, it may be advantageous to have a peatland with a fetch length shorter than that of the flow reattachment distance, as it would increase the ratio of the peatland that is within the sheltered region. Such a configuration would have a higher surface resistance to moisture transfer, limiting potential water losses to an atmosphere with high evaporative demand. Furthermore, gap geometry and FFS shape should be considered during peatland reclamation projects and anthropogenic disturbances as they can influence regional flow dynamics that can alter the evaporative dynamics of surrounding ecosystems.

4.0 Limitations and Conclusions

4.1 Limitations

Edge transition within the simulations were simplified due to the absence of a vegetative buffer zone around the transitions. This simplification has the impact of increasing bleed through flow through the BFS which can increase streamwise velocities within the sheltered region (McNaughton, 1988; Raupach et al., 2001) and through the FFS which can decrease the uplift region of the FFS (Cornelis and Gabriels, 2004; Ruck et al., 2010). This could create bias in the uplift region of our study as it would allow for more canopy dissipation that would reduce the amount of flow being ejected out of the peatland at the FFS (Cornelis and Gabriels, 2004; Ruck et al., 2010). However, it is important to note that the FFS still functions as a displacement height transition while accurately representing an anthropogenic disturbance such as a cut block produced during forestry activities where no buffer region exists.

The horizontal voxel length can result in data bias around the transition edges as the greater turbulence in this region results in a larger portion of the flow being resolved at the sub-grid scale which could decrease the accuracy of the model in these regions. However, the resolved subgrid scale turbulent kinetic energy was less than 1% which is in line with other studies using similar high-resolution voxel sizes (Bohrer et al., 2009). Furthermore, voxel size creates a discretized edge that may create unrealistic flow pattered as the edging around the peatland is resolved as a block and not uniform edge. This has an impact on the representation of flow at the transitions where the flow would follow the blocked edge which could have an impact on the drag and lateral convergence at the transition (Versteeg and Malasekra, 2007). However, at the peatland and regional scale this would most likely be insignificant; however, a smaller size voxel may be needed

if the study primarily focused explicitly on the impact of transition shape (Versteeg and Malasekra, 2007).

Despite the limitation's, difficulty, and assumptions of using a model to make conclusions on turbulent dynamics within complex terrain, the use of a model such as RAFLES gives us greater insight compare to just field measurements. The high resolution of RAFLES allows us to investigate all aspects of the flow compared to single point measurements. Furthermore, models give insight into the processes that govern reality and act as a tool to increase the understanding of natural processes based on the laws of nature, even though it impossible to recreate specific natural time and space instances (Barbour and Krahn, 2004; Refsgaard et al., 2007).

4.2 Conclusions and recommendations

Given the hydrologic sensitivity of the BP, it is critical to understand the implications of turbulent dynamics on moisture transfer rates across as this could influence the hydrologic stability of the peatland of the region. Flow separation produced by displacement height transition results in reduced moisture transfer in the sheltered region while resulting in increased rates in the reattachment followed by an equalization within the recovery region. This results in reduced surface evaporative demand within the sheltered region compared to the reattachment and recovery regions. Increasing the roughness of the peatland surface decreased the variability of evaporative stresses across the surface of the peatland due to the increased turbulence and mixing of moisture. Flow separation has implications for landscape reclamation projects as the spatial distribution of fluxes across a peatland can influence the hydroclimatic stresses and productivity of planted vegetation which could increase the spatial variability of stresses and success of vegetation across the surface. Furthermore, our research shows that rougher surfaces have an overall lower resistance to evaporative demand; however, increasing the surface roughness results in a more uniform

spatial distribution of moisture transfer rates. This could be beneficial in a reclaimed landscape as it would reduce the spatial variability and make the evaporative stresses more predictable across the peatland surface.

Fetch length did not influence the turbulent dynamics of the displacement height transition. That is, the sheltered distance did not change with changes with peatland fetch length. However, the shape of the transition and potentially the geometry of the peatland had implications to regional wind speeds. Funneling of flow within the medium length fetch peatland resulted in faster above canopy streamwise wind velocities compared to the other transition shapes and peatland geometries. FFS shape and gap geometry has implications for forestry practices as cut block forestry create a displacement transition that disrupts flow properties of downwind landscapes. This could change the hydrologic balance of the downwind landscape which can influence the hydroclimatic state of these landscapes. This can also be applied to a reclaimed landscape where peatland geometry and FFS shape should be considered when estimating regional wind velocities in landscape-scale reclamation efforts. For example, in a hypothetical scenario where all peatlands had the same shape and area, it is recommended that the peatlands should variations in their orientations. This would moderate wind velocities and reduce the variations in regional wind velocities based on the wind direction; thereby, making the regional flow more predictable.

5.0 References

Adcroft, A., Hill, C., & Marshall, J. (1997). Representation of topography by shaved cells in a height coordinate ocean model. *Mon Weather Rev*, 125:2293–2315

Admiral, S.W., & Lafleur, P.M. (2007). Partitioning of latent heat flux at a northern peatland. *Aquatic Botany*, 86: 107–116. DOI:10.1016/j. aquabot.2006.09.006

Admiral, S. M., Lafleur, P. M., & Roulet N. T. (2006). Controls on latent heat flux and energy partitioning at a peat bog in eastern Canada. *Agricultural and Forest Meteorology,* 140 308–321

Alberta Environmental Protection. (1998). The boreal forest natural region of Alberta. *Natural Resource Services, Recreation and Protection, Special Report*.

Aubinet, M., Vesala, T., & Papale, D. (2012). *Eddy covariance: a practical guide to measurement and data analysis*. Springer: Dordrecht.

Belcher, S.E., Finnigan, J.J., & Harman, I.N. (2008). Flows through forest canopies in complex terrain. *Ecol Appl,* 18:1436–1453

Belcher, S.E., Harman, I.N., & Finnigan, J.J. (2012). The wind in the willows: flows in forest canopies in complex terrain. *Annu Rev Fluid Mech*, 44(1):479–504

Belcher, S.E., Jerram, N., & Hunt, J.C.R. (2003). Adjustment of a turbulent boundary layer to a canopy of roughness elements. *J Fluid Mech*, 488:369–398

Bergen, J.D., (1975). Air movement in a forest clearing as indicated by smoke drift. *Agric Meteorol,* 15(2):165–179

Betts, A. K., & Ball, J. H. (1997). Albedo over the boreal forest. *Journal of Geophysical Research*, **102**,901– 909

Bohrer, G., Wolosin, M., Brady, R., & Avissar, R. (2007). A virtual canopy generator (V-CaGe) for modeling complex heterogeneous forest canopies at high resolution. *Tellus Ser B Chem PhysMeteorol*, 59:566–576

Bohrer, G., Katul, G., Walko, R., & Avissar, R. (2009). Exploring the effects of microscale structural heterogeneity of forest canopies using large-eddy simulations. *Boundary-Layer Meteorology, 132*(3), 351-382. doi:10.1007/s10546-009-9404-4

Bou-Zeid, E., Meneveau, C., & Parlange, M.B. (2004). Large-eddy simulation of neutral atmospheric boundary layer flow over heterogeneous surfaces: blending height and effective surface roughness. *Water Resour Res*, 40(W02):505. doi:10.1029/2003WR002475

Brown, S.M., Petrone, R.M., Mendoza, C., & Devito, K.J. (2010). Surface vegetation controls on evapotranspiration from a sub humid Western Boreal Plain wetland. *Hydrological Processes*, 24(8): 1072–1085.

Brown, S. M., Petrone, R. M., Chasmer, L., Mendoza, C., Lazerjan, M. S., Landhäusser, S. M., Silins, U., Leach, J., & Devito, K. J. (2014). Atmospheric and soil moisture controls on evapotranspiration from above and within a Western Boreal Plain aspen forest. *Hydrol. Process*, 28: 4449–4462. doi:10.1002/hyp.9879

Brown, S.M., Petrone, R.M., Chasmer, L., Mendoza, C., Lazerjan, M.S., Landhausser, S., Silins, U., Leach, J., & Devito, K.J. (2013). The influence of rooting zone soil moisture on evapotranspiration from above and within a western boreal plain aspen forest. *Hydrol Process*, 28(15): 4449–4462. doi:10. 1002/hyp.9879.

Canadian Oil and Natural Gas Producers. (2018). *Environmental Innovation: Land. Canadian Oil and Natural Gas Producers*. https://www.canadasoilsands.ca/en/environmental-innovation/land#.

Cassiani, M., Katul, G.G., & Albertson, J.D. (2008). The effects of canopy leaf area index on airflow across forest edges: large eddy simulation and analytical results. *Boundary-Layer Meteorol*, 126:433–460

Chapin, F.S., Matson, P.A., & Mooney, H.A. (2002). *Principles of terrestrial ecosystem ecology*. New York: Springer.

Chatziefstratiou, E. K., Velissariou, V., & Bohrer, G. (2014). Resolving the Effects of Aperture and Volume Restriction of the Flow by Semi-Porous Barriers Using Large-Eddy Simulations. *Boundary-Layer Meteorology*, *152*(3), 329-348. Kluwer Academic Publishers.

Cleugh, H.A. (1998). Effects of windbreaks on airflow, microclimates and crop yields. *Agroforestry Systems*, 41: 55. doi:10.1023/A:1006019805109

Cornelis, W.M., & Gabriels, D. (2004). A simple model for the prediction of the deflation threshold shear velocity of dry loose particles. Sedimentology 51, 1–13.

Daly, C., Price, J., Rezanezhad, F., Pouliot, R., Rochefort, L., & Graf, M. D. (2012). Initiatives in oil sand reclamation: Considerations for building a fen peatland in a post-mined oil sands landscape. *Restoration and Reclamation of Boreal Ecosystems*, 179–201.

Damschen, E.I., Baker, D.V., Bohrer, G., Nathan, R., Orrock, J.L., Turner, J.R., Brudvig, L.A., Haddad, N.M., Levey, D.J. and Tewksbury, J.T. (2014). How fragmentation and corridors affect wind dynamics and seed dispersal in open habitats. *Proc. Natl. Acad. Sci. USA.* 111, 3484–3489.

Davis, J. E., & Norman, J. M. (1988). 22. Effects of shelter on plant water use. *Agriculture, Ecosystems and Environment, 22-23*, 393-402.

Detto, M., Katul, G.G., Siqueira, M., Juang, J.H., & Stoy, P.C. (2008). The structure of turbulence near a tall forest edge: the backward facing step flow analogy revisited. *Ecol Appl*, 18:1420–1435

Devito, K. J., Creed, I. F., & Fraser, C. J. D. (2005). Controls on runoff from a partially harvested aspen-forested headwater catchment, Boreal Plain, Canada. *Hydrological Processes*, 19, 3–25.

Devito, K., Mendoza, C., & Qualizza, C. (2012). Conceptualizing water movement in the Boreal Plains. *Implications for watershed reconstruction*, 164.

Dupont, S., & Brunet, Y., (2008a). Edge flow and canopy structure: a large-eddy simulation study. *Boundary-Layer Meteorol*, 126, 51–71.

Dupont, S., & Brunet, Y., (2008b). Impact of forest edge shape on tree stability: a large-eddy simulation study. *Forestry,* 81, 299–315.

Elmes, M. C., Thompson, D. K., Sherwood, J. H., & Price, J. S. (2018). Hydrometeorological conditions preceding wildfire, and the subsequent burning of a fen watershed in Fort McMurray, Alberta, Canada. *Natural Hazards and Earth System Sciences*, 18(1), 157. Retrieved from http://link.galegroup.com.proxy.lib.uwaterloo.ca/apps/doc/A522512059/AONE?u=uniwater&sid=AONE&xid=4fa32057

Ferone, J.M., & Devito, K. J. (2004). Shallow groundwater–surface water interactions in pond–peatland complexes along a Boreal Plain topographic gradient. *Journal of Hydrology*, 292, 75–95.

Finnigan, J. (2000). Turbulence in plant canopies. *Annual Review of Fluid Mechanics,* 32:519–571.

Fontan, S., Katul, G., Poggi, D., Manes, C., Ridolfi, L. (2013). Flume experiments on turbulent flows across gaps of permeable and impermeable boundaries. *Boundary-Layer Meteorol*, 147:21–39

Glime, J.M. (2007). *Bryophyte Ecology. Volume 1. Physiological Ecology. Michigan Technological University and the International Association of Bryologists*, Houghton. http://www.bryoecol.mtu.edu

Global Forest Watch. (2000). Canada's forests at a crossroads: an assessment in the Year 2000. *World Resources Institute*.

Goetz, J.D. & Price, J.S. (2015) Role of morphological structure and layering of Sphagnum and Tomenthypnum mosses on moss productivity and evaporation rates. *Canadian Journal of Soil Science,* 95, 109–124.

Golding, D. L., & Swanson, R. H. (1978). Snow accumulation and melt in small forest openings in Alberta. *Canadian Journal of Forest Research*, 8(4), 380-388. DOI: 10.1139/x78-057

Golubev, V., & Whittington, P. (2018). Effects of volume change on the unsaturated hydraulic conductivity of Sphagnum moss. *Journal of Hydrology*, 559, 884-894. doi:10.1016/j.jhydrol.2018.02.083

Goodine, G.K., Lavigne, M.B., & Krasowski, M.J. (2008). Springtime resumption of photosynthesis in balsam fir (Abies balsamea). *Tree physiology,* 28: 1069–1076.

Goodrick, SL., Achtemeier, G.L., Larkin, N.K., Liu, Y., & Strand, T.M. (2013). Modelling smoke transport from wildland fires: a review. *Int J Wildland Fire,* 22:83–94

Goodrick, S.L., Achtemeier, G.L., Larkin, N.K., Liu, Y., & Strand, T.M. (2013). Modelling smoke transport from wildland fires: a review. *Int J Wildland Fire,* 22:83–94

Gorham, E. (1991). Northern peatlands: role in the carbon cycle and probable responses to climatic warming. *Ecological Applications,* 1: 182–195.

Government of Alberta. (2015). *Alberta's Oil Sands: Reclamation. Government of Alberta*. http://oilsands.alberta.ca/FactSheets/FactSheet-Reclamation-2015.pdf.

Halliwell, D.H., & Rouse, W. R. (1987). Soil heat flux in permafrost: characteristics and accuracy of measurement. *Journal of Climatology,* 7, 571–584.

Heijmans, M., Arp, W.J., & Chapin, F.S.III. (2004). Carbon dioxide and water vapour exchange from understory species in boreal forest. *Agriculutral and Forest Meteorology,* 123: 135–147.

Hokanson, K. J., Lukenbach, M. C., Devito, K. J., Kettridge, N., Petrone, R. M., & Waddington, J. M. (2016). Groundwater connectivity controls peat burn severity in the Boreal Plains. *Ecohydrology*, 9, 574-584 DOI: 10.1002/eco.1657

Irmak, S., & Mutiibwa, D. (2010). On the dynamics of canopy resistance: Generalized linear estimation and relationships with primary micrometeorological variables. *Water Resour. Res.*, 46, W08526, doi:10.1029/2009WR008484.

James, L. (2017). Formation and maintenance of permanent perched wetlands in the Boreal Plain of Western Canada (Unpublished master's thesis). Earth and Atmospheric Sciences, University of Alberta, Edmonton, Alberta, Canada.

Johnson, E.A., & Miyanishi, K. (2008). Creating new landscapes and ecosystems. *Ann. N.Y. Aca. Sci*, 1134, 120–145.

Jones, P., Alexander, D., & Burnett, J. (2004). Pedestrian Wind Environment Around High-Rise Residential Buildings in Hong Kong. *Indoor and Built Environment*, 13(4), 259–269. https://doi.org/10.1177/1420326X04045685

Judd, M. J., Raupach, M. R., & Finnigan, J. J. (1996). A Wind Tunnel Study of Turbulent Flow Around Single and Multiple Windbreaks; Part 1: Velocity Fields, *Boundary-Layer Meteorol*. 80, 127–165.

Ketcheson, S.J., Price, J.S., Petrone, R.M., Sutton, O., Kessel, E.D., & Sutherland, G., (2017). An initial assessment of the hydrological functioning of a constructed fen wetland watershed in the Athabasca Oil Sands region, Alberta, Canada. *Sci. Total Environ*, 603-604 :593–605. :https://doi.org/10.1016/j.scitotenv.2017.06.101.

Kettridge, N., Thompson, D.K., Bombonato, L., Turetsky, M.R., Benscoter, B.W., Waddington, J.M. (2013). The ecohydrology of forested peatlands: simulating the effects of tree shading on moss evaporation and species composition. *Journal of Geophysical Research*, 118:1–14. DOI: 10.1002/jgrg.20043

Kim J, Verma SB. 1996. Surface exchange of water vapour between and open sphagnum fen and the atmosphere. Boundary Layer Meteorology 79: 243–264.

Kljun, N., Calanca, P., Rotach, M., & Schmid, H. (2004). A simple parameterisation for flux footprint predictions. *Boundary-Layer Meteorol*, 112: 503–523. doi:10.1023/B:BOUN.0000030653. 71031.96.

Kondo, J., & Yamazawa, H. (1986). Aerodynamic roughness over an inhomogeneous ground surface. *Boundary-Layer Meteorol*., 35,331-348.

Kuhry, P., Nicholson, B.J., Gignac, L.D., Vitt, D.H., & Bayley, S.E. (1993). Development of Sphagnum-dominated peatlands in boreal continental Canada. *Canadian Journal of Botany*, 71(1): 10-22, https://doi.org/10.1139/b93-002

Lafleur, P.M., & Schreader, C.P. (1994). Water loss from the floor of a sub-arctic forest. *Arctic Alpine Research*, 26: 152–158.

Lee, X. (2000). Air motion within and above forest vegetation in non-ideal conditions. *For Ecol Manag*, 135:3–18

Lettau, H. (1969). Note on aerodynamic roughness-parameter estimation on the basis of roughness-element description. *J. Appl. Meteor.*, 8, 828-832.

Leuning, R. & Judd, M.J. (1996). The relative merits of open and closed path analysers for measurement of eddy fluxes. *Global Change Biology*, 2: 241-253.

Liu, Y.Q., & Avissar, R. (1996). Sensitivity of shallow convective precipitation induced by land surface heterogeneities to dynamical and cloud microphysical parameters. *J Geophys Res*, 101:7477–7497

Loureiro, J. B. R., Monteiro, A. S., Pinho, F. T., & Silva Freire, A. P. (2008). The effect of roughness on separating flow over two-dimensional hills. *Experiments in Fluids*, 46(4), 577–596. doi:10.1007/s00348-008-0583-4

Markfort, C.D., Perez, A.L.S., Thill, J.W., Jaster, D.A., Porte-Agel, F., & Stefan, H.G. (2010). Wind sheltering of a lake by a tree canopy or bluff topography. *Water Resour Res*, 46:W03530

Markfort, C.D., Porté-Agel, F. & Stefan, H.G. (2014). Canopy-wake dynamics and wind sheltering effects on Earth surface fluxes. *Environmental Fluid Mechanics*, 14: 663. doi:10.1007/s10652-013-9313-4

Marshall, I.B., Schut, P., & Ballard, M. (compilers), (1999). Canadian Ecodistrict Climate Normals for Canada 1961–1990. A National Ecological Framework for Canada: Attribute Data. *Environmental Quality Branch, Ecosystems Science Directorate, Environment Canada and Research Branch*, Agriculture and Agri-Food Canada, Ottawa/Hull. DOI: http://sis.agr.gc.ca/cansis/nsdb/ecostrat/district/climate.html.

McCarter, C.P.R., & Price, J.S. (2012). Ecohydrology of *Sphagnum* moss hummocks: mechanisms of capitula water supply and simulated effects of evaporation. Ecohydrology, 7(1), 33-44.

McNaughton, K.G. (1988). Effects of windbreaks on turbulent transport and microclimate. *Agric. Ecosystems Environ.*, 22/23: 17-39.

Metcalfe, R.A., & Buttle, J.M. (1999). Semi-distributed water balance dynamics in a small boreal forest basin. *Journal of Hydrology*, 226: 66–87.

Molder, M., Kellner, E. (2002). Excess resistance of bog surfaces in central Sweden. *Agriculture and Forest Meteorolology*, 112:23–30.

Monin, S., & Obukhov, A. (1954). Basic laws of turbulent mixing in the atmosphere near the ground. *Tr Acad Nauka*, SSR 24:1963–1987

Moore, P. A., Pypker, T. G., & Waddington, J. M. (2013). Agricultural and Forest Meteorology Effect of long-term water table manipulation on peatland evapotranspiration. *Agricultural and Forest Meteorology*, *178–179*, 106–119. https://doi.org/10.1016/j.agrformet.2013.04.013

Mouniemne, S., & Price, J. S. (2007). Seawater contamination of a harvested bog: Hydrological aspects. *Wetlands*, 27: 355-365.

Murphy, H., Chambers, F., & Mceligot, D. (1983). Laterally converging flow. Part 1. Mean flow. J*ournal of Fluid Mechanics*, 127, 379-401. doi:10.1017/S0022112083002785

Murray, C.D., & Buttle, J.M., (2003). Impacts of Clearcut Harvesting on Snow Accumulation and Melt in a Northern Hardwood Forest. *Journal of Hydrology*, 271(1-4): 197-212.

Naidu, S. L., DeLucia, E. H., & Thomas, R. B. (1998). Contrasting pat- terns of biomass allocation in dominant and suppressed loblolly pine. *Can. J. For. Res*. 28, 1116–1124.

Niu, G.Y., Yang, Z.L. (2004). Effects of vegetation canopy processes on snow surface energy and mass balances. *Journal of Geophysical Research*, 109: D23111. DOI:10.1029/2004JD004884

Nwaishi, F., Petrone, R.M., Macrae, M.L., Price, J.S., Strack, M., & Andersen, R. (2016b). Preliminary assessment of greenhouse gas emissions from a constructed fen on postmining landscape in the Athabasca oil sands region, Alberta, Canada. *Ecol. Eng*, 95, 119–128.

Oke, T. R. (1988). *Boundary Layer Climates*. Methuen & Co, Ltd.

Panferov O, SogachevA (2008) Influence of gap size on wind damage variables in a forest. Agric For Meteorol 148:1869–1881

Patton, E.G., Shaw, R.H., Judd, M.J., & Raupach, M.R. (1998). Large-eddy simulation of windbreak flow. *Boundary- LayerMeteorol*, 87:275–306

Patton, E. G., Shaw, R. H., Judd, M. J., & Raupach, M. R. (1998). Large-eddy simulation of windbreak flow. *Boundary-Layer Meteorology*, *87*(2), 275–306. https://doi.org/10.1023/A:1000945626163

Paulson, C. A. (1970). The mathematical representation of wind speed and temperature profiles in the unstable atmospheric surface layer, *J. Appl. Meteorol.*, 9, 857–861, doi:10.1175/1520- 0450(1970)009<0857:TMROWS>2.0.CO;2

Paw, U.K.T., Baldocchi, D.D., Meyers, T.P., & Wilson, K.B. (2000). Correction of eddy-covariance measurements incorporating both advective effects and density fluxes. *Boundary-Layer Meteorol*, 97:487–511

Pepin, S., Plamondon, A., & Britel, A. (2002). Water relations of black spruce trees on a peatland during wet and dry years. *Wetlands, 22*(2), 225-233. doi:10.1672/0277-5212(2002)022[0225:WROBST]2.0.CO

Petrone, R.M., Chasmer, L., Hopkinson, C., Silins, U., Landhäusser, S.M., Kljun, N., & Devito, K.J. (2015). Effects of harvesting and drought on CO2 and H2O fluxes in an aspen-dominated western boreal plain forest: early chronosequence recovery. *Canadian Journal of Forest Research*, 45(1): 87–100.

Petrone, R. M., Rouse, W. R, & Marsh, P. (2000). Comparative surface energy budgets in western and central subarctic regions of Canada. *International Journal of Climatology*. https://doi.org/10.1002/1097-0088(200008)20:10<1131::AID-JOC524>3.0.CO;2-J

Petrone, R. M., U. Silins, & K. J. Devito. (2007). Dynamics of evapotranspiration from a riparian pond complex in the Western Boreal Forest, Alberta, Canada. *Hydrolgocial Processes*, 21, 1391- 1401.

Petrone, R.M., Smith, C., Macrae, M.L., & English, M.C. (2006). Riparian zone equilibrium and actual evapotranspiration in a 1st order agricultural catchment in Southern Ontario, Canada. *Agric. Water Manag*. 86, 240–248.

Petrone, R.M., Waddington, J. M., & Price, J.S. (2001). Ecosystem scale evapotranspiration and net CO2 exchange from a restored peatland. *Hydrological Processes*, 10.1002/hyp.475

Plach, J. M., Petrone, R. M., Waddington, J. M., Kettridge, N., & Devito, K. J. (2016). Hydroclimatic influences on peatland CO2exchange following upland forest harvesting on the Boreal Plains. *Ecohydrology*, *9*(8), 1590–1603. https://doi.org/10.1002/eco.1750

Price, J.S. (1997). Soil moisture, water tension, and water table relationships in a managed cutover bog. *Journal of Hydrology*, 202: 21–32.

Prueger, J.H., Eichinger, W.E., Hipps, L.E., Hatfield, J.L., & Cooper, D.I. (2008). Air-flow distortion and turbulence statistics near an animal facility. *Atmos Environ*, 42:3301–3314

Raupach, M.R., Finnigan, J.J., & Brunet, Y. (1996). Coherent eddies and turbulence in vegetation canopies: the mixing-layer analogy. *Bound.-Layer Meteorol*. 78, 351±382.

Riddell, J. F. (2008). Assessment of surface – groundwater interactions at perched boreal wetlands, north-central Alberta (Unpublished master's thesis). Earth and Atmospheric Sciences, University of Alberta, Edmonton, Alberta, Canada.

Rooney, R.C., Bayley, S.E., & Schindler, D.W. (2012). Oil sands mining and reclamation cause massive loss of peatland and stored carbon. *Proc. Natl. Acad. Sci*. doi: http://dx.doi.org/10.1073/pnas.1117693108.

Ruck, B., Frank, C., & Tischmacher, M. (2012). On the influence of windward edge structure and stand density on the flow characteristics at forest edges. *Eur J For Res*, 131:177–189

Runkle, B. R. K., Wille, C., Gažovič, M., Wilmking, M., & Kutzbach, L. (2014). The surface energy balance and its drivers in a boreal peatland fen of northwestern Russia. *Journal of Hydrology, 511*(Complete), 359-373. doi:10.1016/j.jhydrol.2014.01.056

Rydin, H., & J. K. Jeglum. (2006). The Biology of Peatlands. Oxford University Pres., New York.

Schipperges, B., & Rydin, H. (1998). Response of photosynthesis of Sphagnum species from contrasting microhabitats to tissue water content and repeated desiccation. *New Phytologist*, 140: 677–684.

Simpson, R. (1989). Turbulent boundary layer separation. *Ann Rev Fluid Mech*, 21:205–234

Solondz, D.S., Petrone, R.M., & Devito, K.J. (2008). Forest floor carbon dioxide fluxes within an upland peatland complex in the Western Boreal Plain, Canada. *Ecohydrology*, 1(4): 361–376.

Sonnentag, O., J. M. Chen, D. A. Roberts, J. Talbot, Halligan, K. Q., & Govind, A. (2007). Mapping tree and shrub leaf area indices in an ombrotrophic peatland through multiple endmember spectral unmixing. *Remote sensing of Environment*, 109, 342-360.

Strack, M., & Price, J.S. (2009). Moisture controls on carbon dioxide dynamics of peat-Sphagnum monoliths. *Ecohydrology*, 2: 34–41. DOI: 10.1002/eco.36.

Strack, M., Waddington, J. M., Lucchese, M. C., & Cagampan, J. P. (2009). Moisture controls on CO2 exchange in a Sphagnum-dominated peatland: Results from an extreme drought field experiment. *Ecohydrology*, *2*(4), 454-461. doi:10.1002/eco.68

Strilesky, S.L., & Humphreys, E.R. (2012). A comparison of the net ecosystem exchange of carbon dioxide and evapotranspiration for treed and open portions of a temperate peatland. *Agricultural and Forest Meteorology*, 153:45–53.

Sutherland, G., Chasmer, L. E., Kljun, N., Devito, K. J., & Petrone, R. M. (2017). Using High Resolution LiDAR Data and a Flux Footprint Parameterization to Scale Evapotranspiration Estimates to Lower Pixel Resolutions. *Canadian Journal of Remote Sensing*, *43*(2), 215–229. https://doi.org/10.1080/07038992.2017.1291338

Thompson, D. K., Baisley, A. S., & Waddington, J. M. (2015). Seasonal variation in albedo and radiation exchange between a burned and unburned forested peatland: Implications for peatland evaporation. *Hydrological Processes*, **29**, 3227– 3235.

Timoney, K.P. (2003). The changing disturbance regime of the boreal forest of the Canadian Prairie Provinces. *The Forestry Chronicle*, 79(3): 502–516.

Troendle, C. A., & Leaf, C. F. (1980). Hydrology, An Approach to Water Resource Evaluation of Non-Point Silvicultural Source. *Environ. Prot. Agency (US), Publ., Ap. Ser*, 60018-012.

Turetsky, M.R., Kane, E.S., Harden, J.W., Ottmar, R.D., Manies, K.L., Hoy, E., & Kasischke, E.S. (2011). Recent acceleration of biomass burning and carbon losses in Alaskan forests and peatlands. *Nat. Geosci*, 4 (1), 27–31.

Van der Kindere, J., & Ganapathisubramani, B. (2018). Effect of length of two-dimensional obstacles on characteristics of separation and reattachment. *J Wind Eng Ind Aerodyn*, 178:38–48

Vasander, H., & Kettunen, A., (2006). Carbon in boreal peatlands. In: Wider, R.K., Vitt, D.H. (Eds.), Boreal Peatland Ecosystems. *Springer-Verlag*, Heidelberg, Germany, pp. 165–194.

Vitt, D.H., Bayley, S.E., & Tai-Long, J. (1995). Seasonal variation in water chemistry over a bog-rich fen gradient in continental western Canada. *Canadian Journal of Fisheries and Aquatic Science*, 52: 587–606.

Vitt, D., Halsey, L., Thormann, M., & Martin, T. (1996). Peatland inventory of Alberta. Phase 1: Overview of peatland resources in the natural regions and subregions of the province., Centre PR (ed.) University of Alberta.

Vogel, J.C., & Eaton, J.K. (1985). Combined heat-transfer and fluid dynamic measurements downstream of a backward-facing step. *J Heat Transf Trans ASME*, 107:922–929

Waddington, J.M., Morris, P.J., Kettridge, N., Granath, G., Thompson, D.K., & Moore, P.A. (2015). Hydrological feedbacks in northern peatlands. *Ecohydrology*, 113– 127. http://dx.doi.org/10.1002/eco.1493.

Wang, H., & Takle, E.S. (1997). Momentum budget and shelter mechanism of boundary layer flow near a shelterbelt. *Boundary-Layer Meteorol*, 82: 417–435

Wang, H., & Takle, E. S. (1995). Boundary-Layer Flow and Turbulence Near Porous Obstacles. I. Derivation of a General Equation Set for a Porous Medium, *Boundary-Layer Meteorol,* 10.1007/BF00715711

Webb, E.K., Pearman, G., & Leuning, R. (1980). Correction of flux measurements for density effects due to heat and water vapour transfer. *Quarterly Journal of the Royal Meteorology Society*, 106: 85–100.

Wilson, K., Goldstein, A., Falge, E., Aubinet, M., Baldocchi, D., Berbigier, P., Bernhofer,C., Ceulemans, R., Dolman, H., Field, C., Grelle, A., Ibrom, A., Law, B.E., Kowalski, A.,Meyers, T., Moncrieff, J., Monson, R., Oechel, W., Tenhunen, J., Valentini, R., & Verma, S. (2002). Energy balance closure at FLUXNET sites. *Agric. Forest Meteorol*. 113,223–243.

Yang, B., Morse, A., Shaw, R., & Paw, U.K.T. (2006b). Large-eddy simulation of turbulent flow across a forest edge. Part II: momentum and turbulent kinetic energy budgets. *Boundary-Layer Meteorol,* 121:433–457

Yang, B., Raupach, M., Shaw, R.H., Paw, U.K.T., & Morse A.P. (2006a). Large-eddy simulation of turbulent flow across a forest edge. Part I: flow statistics. *Boundary-Layer Meteorol*, 119:377–412. doi:10.1007/ s10546-006-9083-3

Yue, W., Parlange, M.B., Meneveau, C., Zhu, W., vanHout, R., & Katz, J. (2007). Large-eddy simulation of plant canopy flows using plant-scale representation. *Boundary-Layer Meteorol*, 124(2):183–203

Appendix

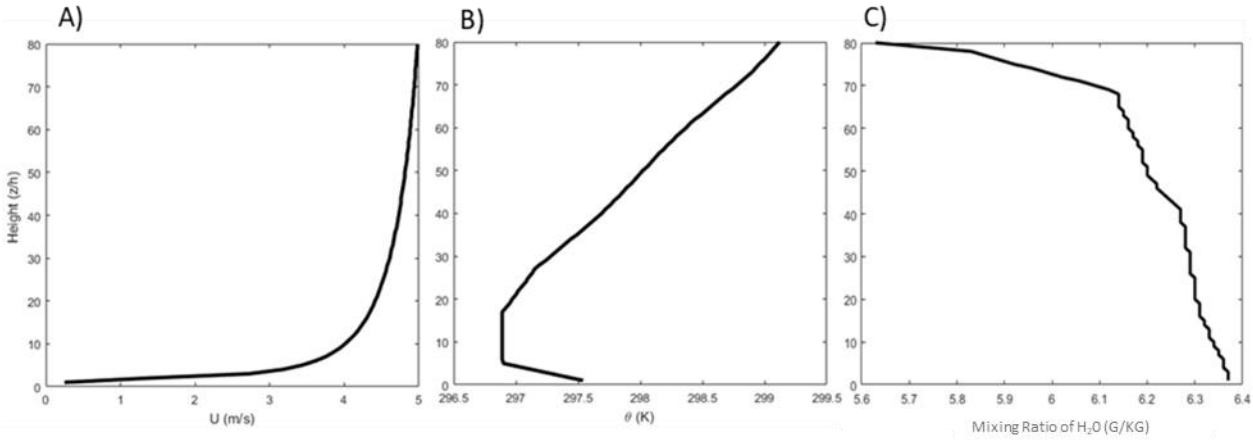

Figure A-1: A) Wind speed profiles calculated using equation 1, as determined from a single point measurement in (m/s). B) Vertical profile used to prescribe RAFLES with potential temperature in (K) for all cases. C) Vertical profile used to prescribe RAFLES with mixing ratio in grams of H_2O per kilogram of air for all cases.

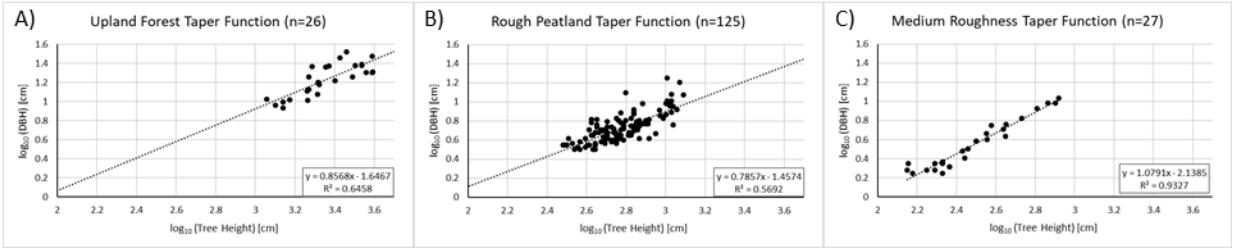

Figure A-2: Trunk taper functions used to parameterize V-CaGe: A) Upland forest B) Rough peatland C) Medium peatland.

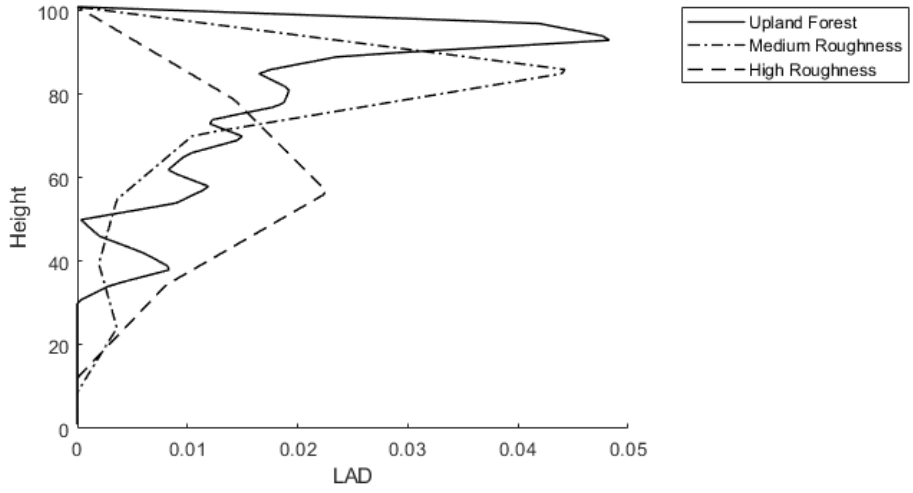

Figure A-3: LAD Profiles created by V-CaGe and used in RAFLES for the prescribed canopy.